Advanced Materials

IIM
Metallurgy
Materials Engineering

The Indian Institute of Metals

All for a better quality of life

As a steel major, we are conscious of our role in India's fast forward industrial drive.

What we also consider with equal concern is the upliftment of the less fortunate people around us.

Under the banner of **Corporate Social Responsibility**, we put in our little big efforts for the community living around the plant, efforts that are designed to ensure a better quality of life for them.

Health care, education, occupation and industrial training including those for the handicapped, self-reliance through indirect employment, development of village infrastructure, recreation facilities are some of the areas we are concentrating on…A soul satisfying experience that we are committed to enhancing as we move along.

स्टील अथॉरिटी ऑफ इण्डिया लिमिटेड
STEEL AUTHORITY OF INDIA LIMITED

Durgapur Steel Plant
Durgapur – 713 203, West Bengal, India

SOBHAGYA

CONTENTS

Cover courtesy : https://st.llnl.gov/node/63
&
https://www.timeshighereducation.com/sites/default/files/advanced_materials_and_manufacturing_375x211.jpg

Chief Editor : Dr N Eswara Prasad

THE INDIAN INSTITUTE OF METALS

Ultra High Temperature Ceramics as a Thermal Protection System of a Hypersonic Vehicle

Manish Patel

Abstract

In hypersonic vehicles, a hot-structure-based sharp thermal protection system offers enormous potential to improve performance. However, at the point of stagnation, the acute hot structure has a very high surface temperature. Due to their high melting point and thermal conductivity, as well as the high melting point of their oxide products, ZrB_2- and HfB_2-based ultrahigh temperature materials are prospective materials to withstand the intense heat on the surface of sharp hot structures (ZrO_2 and HfO_2). Furthermore, adding SiC (10-30% by volume) to ZrB_2 and HfB_2 improves oxidation resistance as well as mechanical qualities, allowing them to withstand thermal and aerodynamic stress during flight. For extended durations of testing in a hypersonic environment, ZrB_2 and HfB_2-based composites outperformed currently utilised materials for hot structures (such as C/C and C-SiC composites).

Keywords : Hypersonic, Hot structure, Zirconium diboride, Thermal conductivity, Strength.

1. Hypersonic flights

The severe circumstances associated with hypersonic flying [1] have aroused the curiosity of aerodynamics researchers. When the flight has a Mach number greater than 5, the flow is considered hypersonic. The vehicle's aerodynamic surface heats up significantly in such flow. The nose cap, engine cowl inlets, and the leading edges of the wings are the parts of the hypersonic vehicle that are most affected. Figure 1 depicts a proposed air-breathing hypersonic vehicle with several affected components. Figure 2 shows the surface temperature of these components during hypersonic flow at 80,000 feet with the flying Mach number. The surface temperature rises as the Mach number rises [2]. Three types of thermal management techniques are available to minimise such high surface temperatures during hypersonic flight [3]; active cooling, semi-passive, and passive thermal management are the three types (Fig.3). The surface heat is carried away from the surface by a constant flow of fluid in active cooling (transpiration, film, and convective cooling) [1, 3]. Heat pipes and ablation are the two types of semi-passive thermal management systems [1, 3]. Passive thermal management, on the other hand, employs heat sink structures, hot structures, and insulated structures [1, 3]. As shown in Fig.4, Bertin et al. [1] described the feasible thermal management concept. For longer duration flights, active cooling is used for high heat flux. However, switching from passive to active cooling for thermal management increases the cost, complexity, and weight of the hypersonic vehicle. As a result, passive thermal management are normally preferred to active and semi-active cooling for improved hypersonic vehicle performance. Furthermore, because of the larger transverse range and mobility, as well as soft re-entry trajectories, a hypersonic vehicle with sharp hot-structure based leading edges will have lower aerodynamic drag and improved flight performance [4-5].

2. Hot structure thermal management

The overall heat flux in a hot structure is constant (Fig. 5). A bow shock arises in front of the tip in hypersonic flow, and gases travelling through it are compressed, increasing density, pressure, static enthalpy, and temperature [4]. The heat
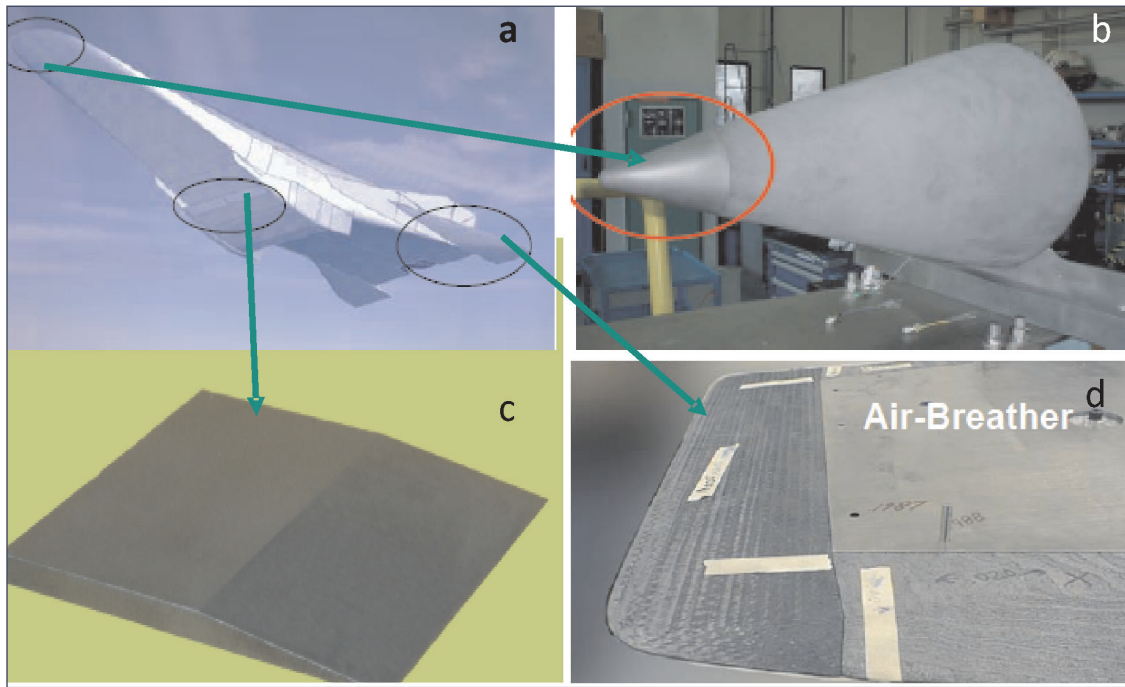
Fig. 1 : (a) A conceptual air-breathing hypersonic vehicle [12], (b) Nose cap, (c) Engine cowl inlets & (d) Wing leading edges [3]
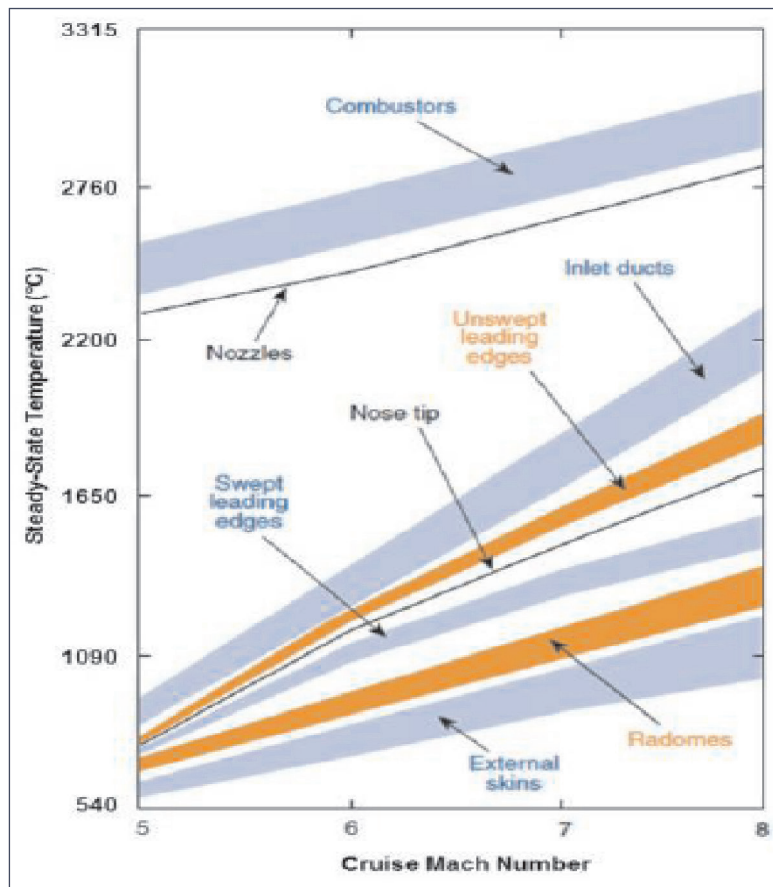
Fig. 2 : Effect of velocity of flight on the surface temperature due to aerodynamics heating [2]
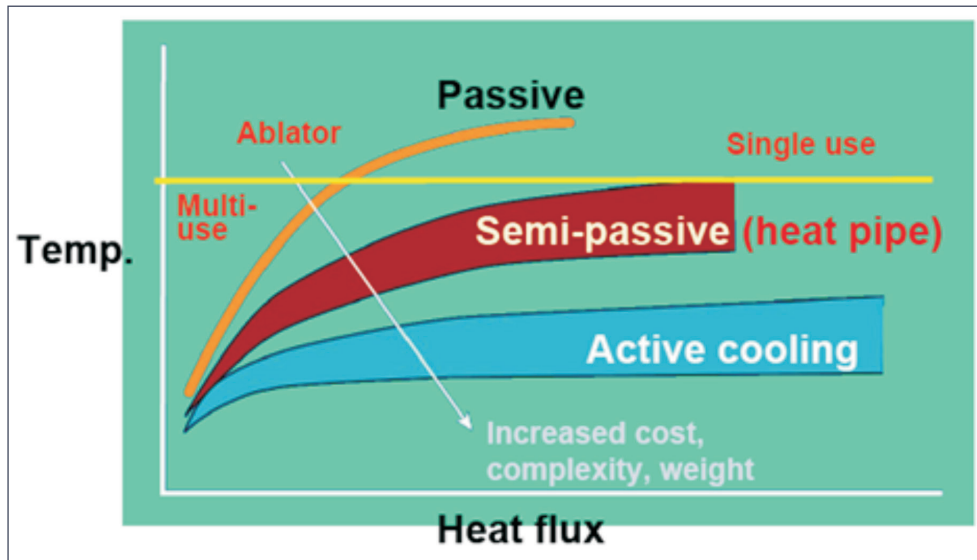
Fig. 3 : Thermal management options for thermal protection of a hypersonic vehicle
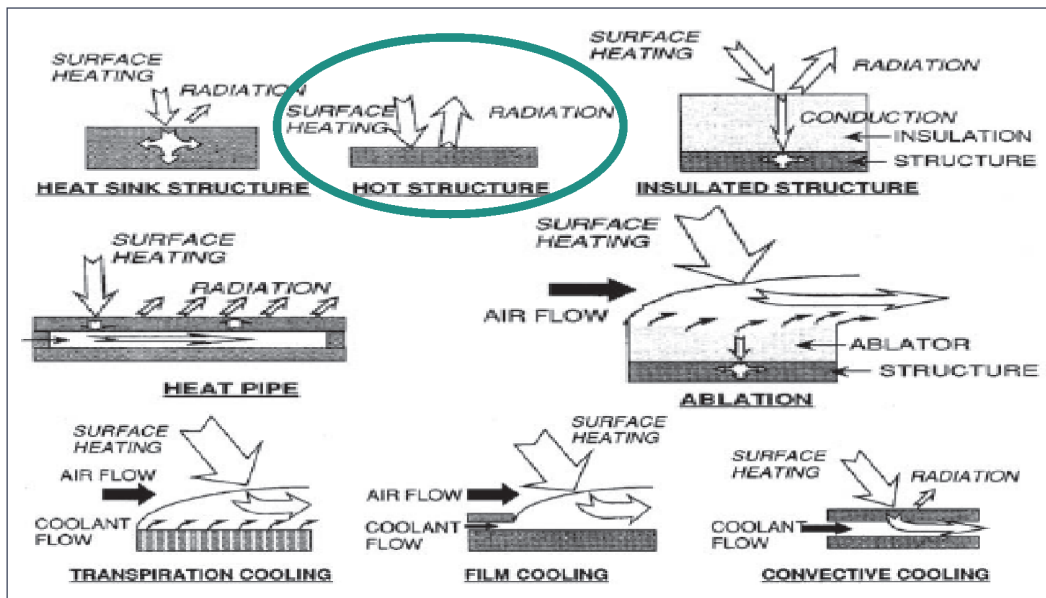
Fig. 4 : Thermal management concept for the thermal protection system for a hypersonic flight [4]

input in hypersonic flow comes from both convective heat energy of gases and chemical energy from exothermic recombination of O and N atoms as N_2 and O_2 molecules dissociate into atoms during passing the bow shock [6]. Part of the heat is reflected back into the environment, while the rest is carried away from the stagnation zone. During hypersonic flow, this results in a constant state equilibrium temperature on the surface of the hot structure. The following energy balance at the surface can be used to compute the steady state equilibrium surface temperature [7].

$$Q_{conv} + Q_{chem} = Q_{rad} + Q_{cond} \quad (1)$$

The following equation gives the heat flux (Q_{conv}) due to convective heat energy of gases. [8].

$$Q_{conv} = (3.88 \times 10^{-4}) \left(\sqrt{\frac{p}{r}}\right) (h_{aw} - h_w) \quad (2)$$

Where p is the overall pressure behind the bow shock and r is the component's radius of curvature. The adiabatic wall enthalpy and the air enthalpy are represented by h_{aw} and h_w, respectively. The heat flow (Q_{chem}) due to N and O recombination

can be calculated using the following equation [7].

$$Q_{chem} = \sum_i y' T \Delta E_i n_i \sqrt{\frac{RT}{8\pi M_i}} \quad (3)$$

$$i = O \ \& \ N$$

Where E represents molecular dissociation energy, n represents atom number densities above the surface, M represents the molar mass, R represents the universal gas constant, T represents surface temperature, and y represents total catalytic efficiency. Equations (4) and (5) yield the heat flux radiated back to the environment (Q_{rad}) and heat conducted away from stagnation (Q_{cond}) respectively.

$$Q_{rad} = \varepsilon \times \sigma \times (T^4 - T_\infty^4) \quad (4)$$

$$Q_{cond} = -K \times \frac{dT}{dx} \quad (5)$$

Where ε is emissivity, σ is the Stefan-Boltzmann constant, and K is the material's thermal conductivity. T stands for the ambient temperature in Kelvin Equation (1) predicts the steady state surface temperature on the hot structure of a hypersonic flight by combining equations (2) to (4). By considering an insulated hot structure (Q_{cond}=0), the maximum surface temperature (also known as radiation equilibrium temperature [4, 9]) can be computed. At a flight speed of 20 Mach number and a material emissivity of 0.5, the maximum attainable surface temperature for a hot structure with a radius of curvature of 25.4 mm is predicted to reach around 3700 ^{0}C (Fig. 6a) [9]. When the heated structure is sharp, the maximum feasible surface temperature exceeds the highest known melting point of materials. At a flying speed of 10 Mach number, the maximum feasible surface temperature for a heated structure with a radius of curvature of 2.54 mm is predicted to be around 4700 ^{0}C (Fig.6b [9]). Heat flux varies inversely with the square root of the nose radius [3, 10], as is well known in aerodynamic heating. Figure 7 depicts the heat flux as a function of radius, revealing that the heat flux is 500 W/cm^2 with a 10 mm tip radius at a specific aerodynamic condition [3]. The heat flux increases dramatically as the radius gets smaller (which is essential for sharp leading edge hypersonic vehicles). As a result of the smaller curvature radius, the surface temperature of the blunt vehicles is higher.

3. Material properties requirement for sharp hot structure

High melting point, thermal conductivity, emissivity, and poor catalytic effectiveness for recombination of O and N are the primary selection criteria for an efficient material to withstand the high surface temperature of a hot structure with severe curvature. Figure 8 shows the melting point and density of possible materials with very high melting points [11]. It indicates that ZrB_2, HfB_2, HfC, ZrC, TaC, TiB_2, TiC, NbC, and other refractory metals (indicated in green circle) have melting points greater than 3000 ^{0}C, as do some refractory metals such as W, Re, Ta, and Os. These materials oxidise in an oxidative environment, forming a surface oxide layer. Oxides should have a melting point greater than the application temperature to maintain structural integrity. The temperature rise in this severe environment could reach 2000 ^{0}C [4, 12]. The condensed phase stability diagram (Fig. 9) of these refractory metals
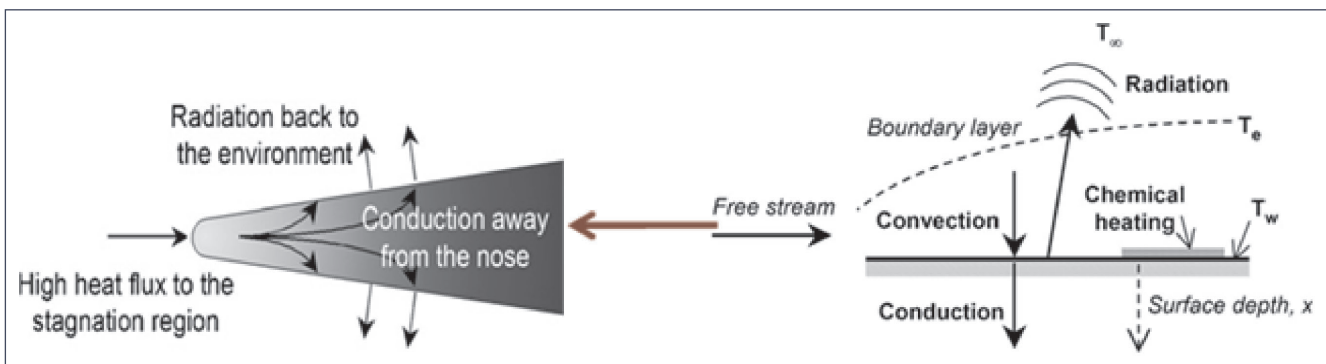
Fig. 5 : Mode of the heat transfer for hot structure based thermal protection system [1]
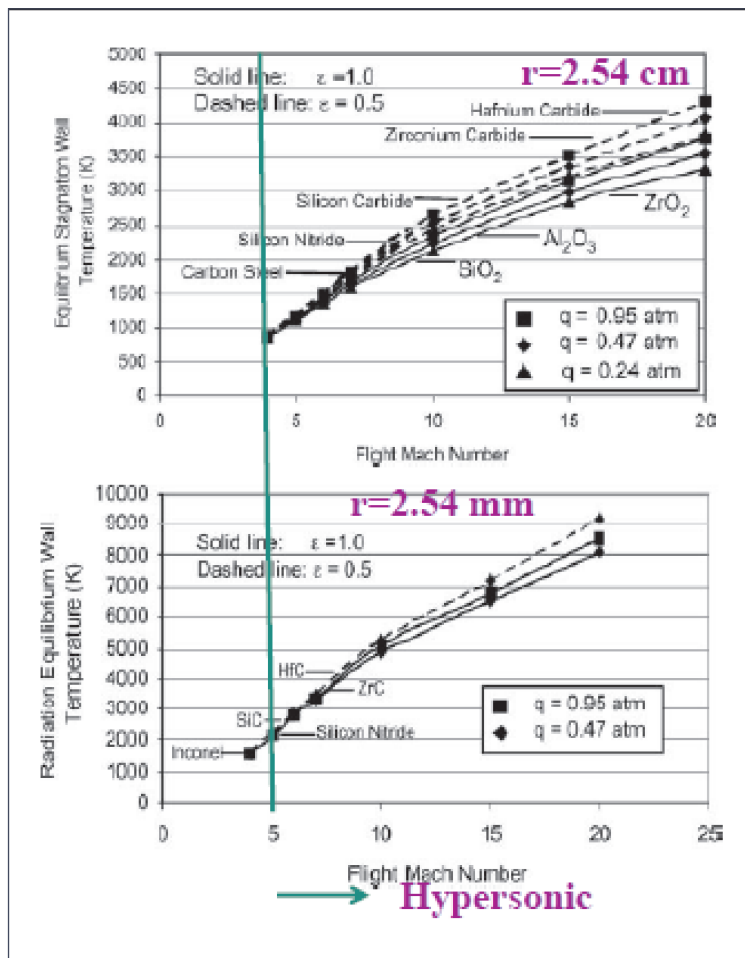
Fig. 6 : The calculated maximum possible surface temperature (Radiation equilibrium temperature) on the hot structure [9]
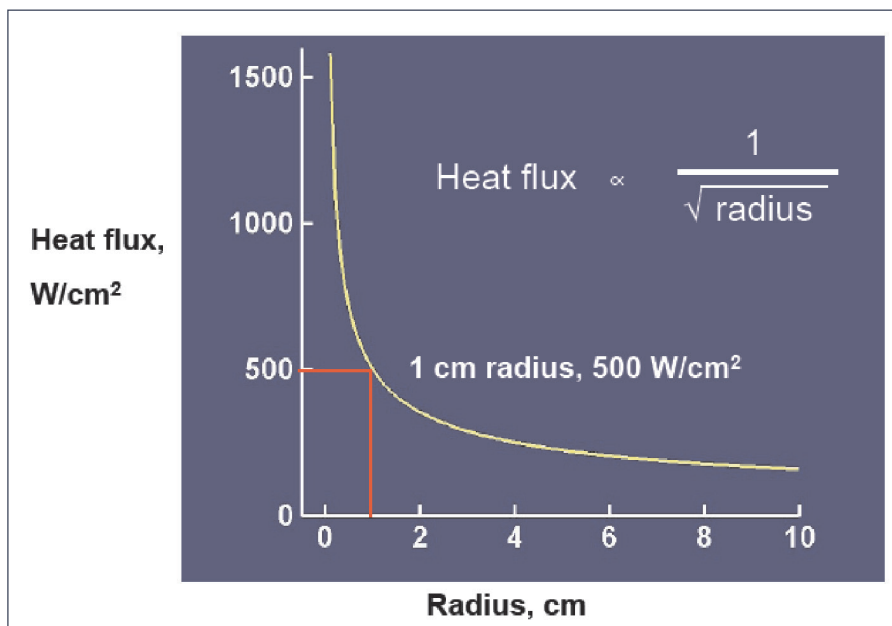
Fig. 7 : Effect of radius of curvature on convective heat flux on the surface of thermal protection system [2]
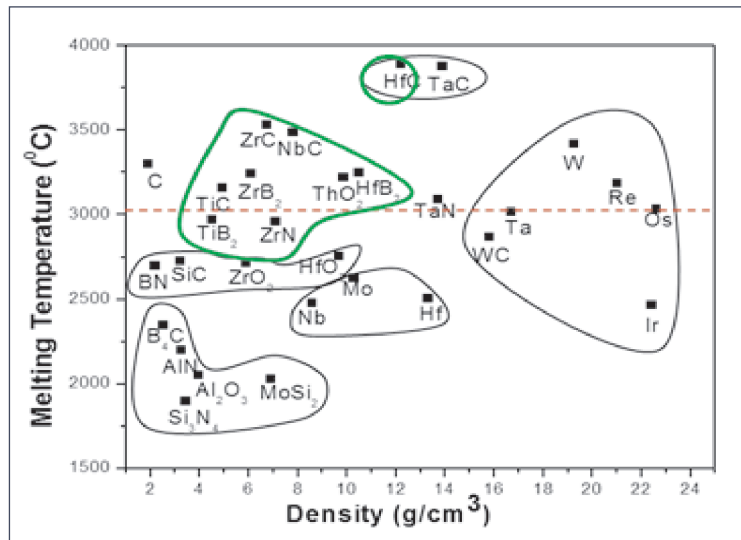
Fig. 8 : Melting point vs. density plot of high melting point materials [11]
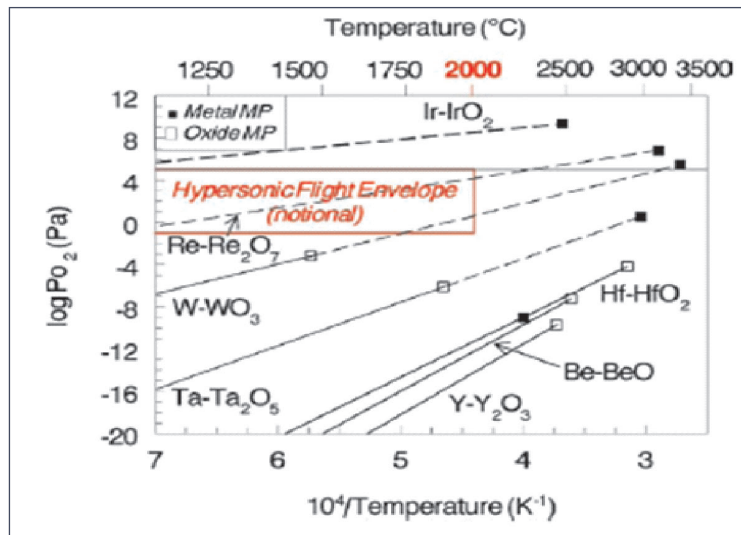
Fig. 9 : Metal-metal oxide condensed phase equilibrium diagram [13]

reveals that either their oxides have melting temperatures below 2000 ^{0}C (i.e. WO_3, Re_2O_7, and Ta_2O_5) or they have a substantial mass loss due to the presence of volatile oxides [13]. Iridium is a unique noble metal with a melting point of ~2500 ^{0}C and relatively little mass loss due to oxidation [13]. Figure 10 shows the relationship between melting point and density for the materials listed above, as well as their oxides [11]. Only ZrO_2 and HfO_2 have melting points exceeding 2000 ^{0}C. Actual experiments support the aforementioned analogy (Fig. 11). After 3 minutes of exposure at temperatures greater than 2000 ^{0}C (arc jet testing), optical micrographs of HfC and TaC

reveal the existence of dense and adhering HfO_2 scale on HfC and signs of residual molten Ta_2O_5 on TaC (Figure 11) [14]. TaC, despite having a melting point similar to HfC [14], cannot be employed for the aforementioned application. Some oxides, like ThO_2, BeO, MgO, CaO, Cr_2O_3, La_2O_3, Y_2O_3, ZrO_2, HfO_2, are stable in oxidising environments above 2000 ^{0}C and could be used as ultra high temperature ceramics (UHTCs). However, because MgO, CaO, and Cr_2O_3 have significant evaporation rates and La_2O_3, Y_2O_3, MgO, and CaO are hygroscopic, the structural integrity of these oxides at very high temperatures is likely to be poor [15]. ThO_2 is radioactive, but BeO is poisonous [15]. The solid

state phase-shift of ZrO_2 and HfO_2 occurs with a substantial volume change [15]. Apart from these drawbacks, these oxides have a limited heat conductivity, making them unsuitable for the aforementioned purposes. As a result, Zr and Hf based carbides and borides are two of the few materials that could be used in ultra-high temperature structural applications. Borides are preferred over carbides because carbides are more brittle and have lower thermal conductivity.

4. ZrB_2 based ultra high temperature ceramics

The design of a thermal protection system based on a hot structure is based on two criteria.

(1) The component's surface temperature and temperature gradient

(2) Thermal stress caused by temperature gradient across thickness.

Thermal conductivity, emissivity, and catalytic efficiency of oxygen and nitrogen recombination are three parameters of ZrB_2 and HfB_2 that must be considered in order to forecast surface temperature and temperature gradients in the component.

4.1. Properties needed for predicting the surface temperature as well as the temperature gradient

4.1.1. Thermal conductivity

In order to reduce peak surface temperatures, improve thermal shock resistance, and reduce internal stress in hot structures, high thermal conductivity is necessary. Carbon-carbon composites and carbon fibre reinforced SiC-composites are currently used for the hot structure of hypersonic aircraft. At normal temperature, these materials have a thermal
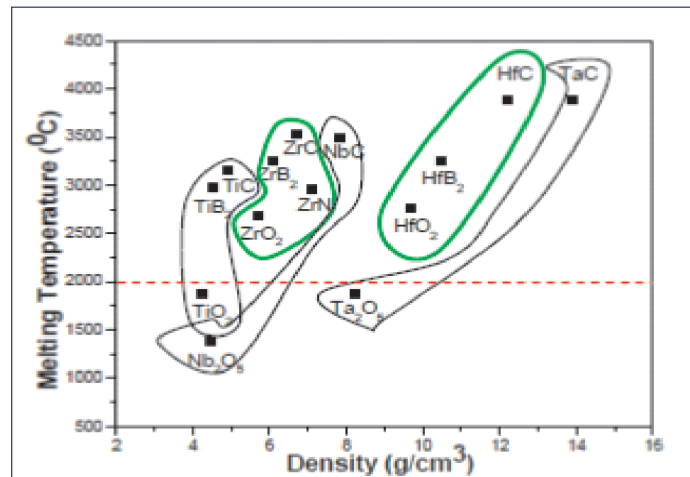
Fig. 10 : Melting point vs. density plot of very high meting materials with their oxide products [11]

Fig. 11 : Optical micrographs of HfC and TaC after 3 minute exposure at T > 2000 ^{0}C [14]

conductivity of 40-60 Wm^{-1} K^{-1} (Fig. 12). C/C composites have a thermal conductivity of 50 W m^{-1}K^{-1} at 1200 ^{0}C [16], but SiC-based materials lose thermal conductivity at high temperatures [17]. Only pitch-based C/C composites have exceptionally high thermal conductivity (233 W m^{-1} K^{-1} at ambient temperature and 85 W m^{-1} K^{-1} at 1500 ^{0}C [16]).The thermal conductivity of ZrB$_2$ and HfB$_2$ composites, on the other hand, is substantially higher than that of C/C and C-SiC composites. At normal temperature, single crystal ZrB$_2$ has thermal conductivities of 140 Wm^{-1}K^{-1} and 100 Wm^{-1}K^{-1} along the a and c axes, respectively [18]. The thermal conductivity of hot pressed monolithic ZrB$_2$ at room temperature is determined to be 85 Wm^{-1}K^{-1} (figure 13) [19]. ZrB$_2$ also maintains its strong thermal conductivity at high temperatures (from room temperature to 1500 ^{0}C, 10 W m^{-1} K^{-1} [19]). It's most likely owing to ZrB$_2$'s electronic-dominated heat conduction mechanism [19]. The addition of SiC to ZrB$_2$ as reinforcement improves oxidation resistance by allowing the creation of a protective top SiO$_2$ rich glassy oxide layer [20]. When SiC is added to ZrB$_2$, the ZrB$_2$-SiC composite has a higher thermal conductivity at room temperature than that of monolithic ZrB$_2$. (figure 13). At high temperatures, however, the thermal conductivity of ZrB$_2$-SiC composite is lower than monolithic ZrB$_2$ (figure 13). As an essential attribute is thermal conductivity, the precision of the thermal conductivity value reduces uncertainty in surface temperature and stress gradient prediction in hot structures. However, the reported thermal conductivity values of ZrB$_2$ and HfB$_2$-based materials exhibit a wide range of values as well as a temperature dependence. Figure 14a depicts the thermal conductivity of ZrB$_2$ and ZrB$_2$-SiC composites, which demonstrates variety in values as well as reliance on temperature and SiC content. Similarly, Gasch et al. [25] discovered that the thermal conductivity of a HfB$_2$-20 percent SiC composite varies by a factor of three at ambient temperature (Fig.14b).

As heat conduction from the stagnation point reduces due to the development of oxides, the surface temperature of a hot structure may change due to oxidation. The arc jet testing of HfB$_2$-SiC composite [26] demonstrates this. The rise in temperature during the last 400 seconds of the first exposure, as indicated in Fig.15a, and a significantly greater temperature following the second exposure is due to oxidation. The production of oxide scale causes a drop in the heat conductivity of the ZrB$_2$- SiC composite. Figure 15b shows the temperature response of the exposed sample versus the unexposed sample. To get varied oxide thicknesses, the exposure was car ried out for 5 hours at 1000 ^{0}C, 1500 ^{0}C, and 1700 ^{0}C [20].The thermal conductivity of ZrB$_2$-SiC composite was reduced due to the formation of thicker oxide scale after exposure at 1500 ^{0}C and 1700 ^{0}C for 5 hours [27].
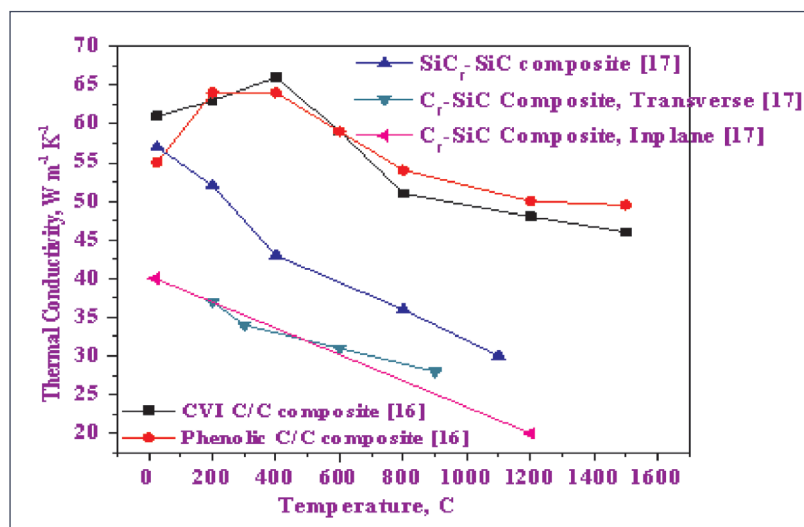
Fig. 12 : Thermal conductivity vs temperature plot of currently used materials for hot structure based thermal protection system in hypersonic vehicle
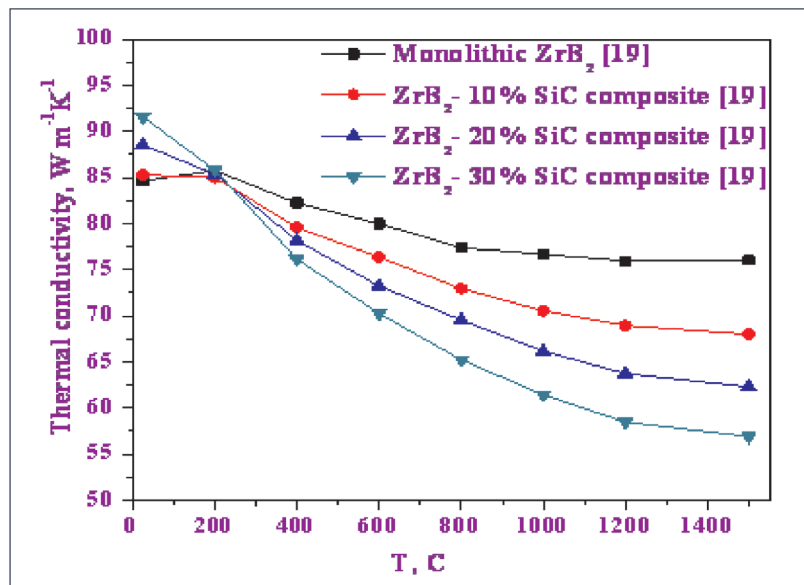
Fig. 13 : Thermal conductivity of monolithic ZrB_2 and ZrB_2- SiC composite at high temperature [19]
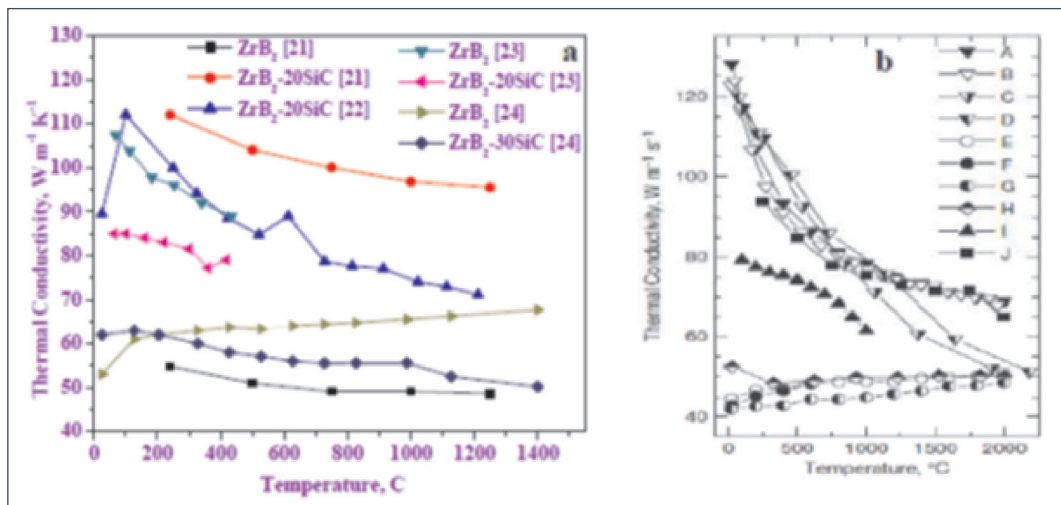
Fig. 14 : The variability in the thermal conductivity as reported in literature, (a) ZrB_2 based materials [19] and (b) HfB_2 based material [25].

4.1.2. Emissivity

To minimise the surface temperature of a heated structure, a high emissivity value is ideal. C/C and C-SiC composites (currently utilised materials for hot structure) have extremely high emissivity [28]. Figure 15 shows the emissivity of C/C and C-SiC composites as a function of temperature. With increasing temperature, the emissivity of C/C and coated C-SiC composites diminishes. The emissivity of uncoated C-SiC composite, on the other hand, follows the opposite pattern. In addition, the emissivity of the uncoated C-SiC

composite is higher than that of the coated C-SiC composite. C/C and C-SiC composites exhibit similar emissivity values when made using ZrB_2-based materials (Figure 16). At lower temperatures, the emissivity values of ZrB_2-SiC composite are more scattered than at higher temperatures. Between 1200 and 1600 ^{0}C, the emissivity of ZrB_2-SiC composite is 0.75 to 0.8 [29-32]. The creation of a separate layer of SiO_2 rich oxide scale owing to oxidation of the ZrB_2-SiC composite may result in a lower scatter value of emissivity at high temperatures. The top layer of SiO_2 rich oxide scale also contains
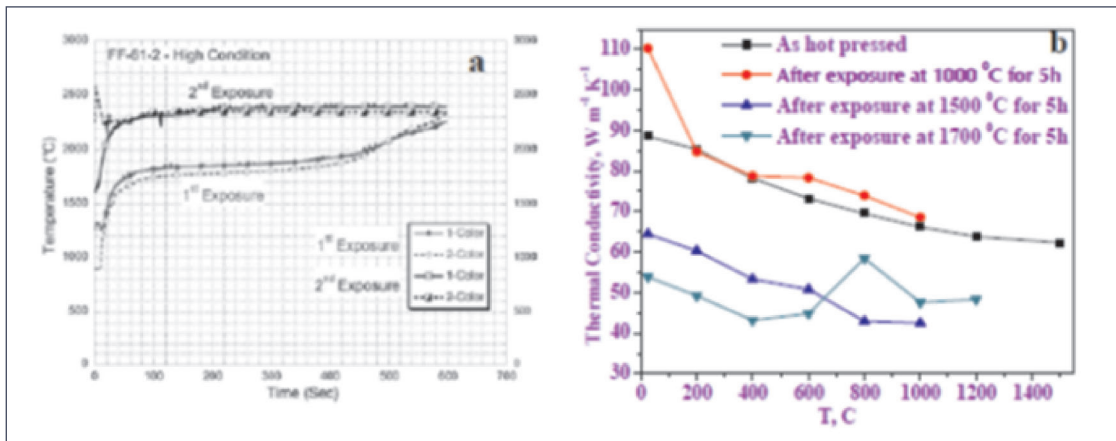
Fig. 15 : Effect of oxide scale build on (a) the surface temperature of hot structure made of HfB$_2$ based composite [26] & (b) thermal conductivity of ZrB$_2$ – SiC composite [27]
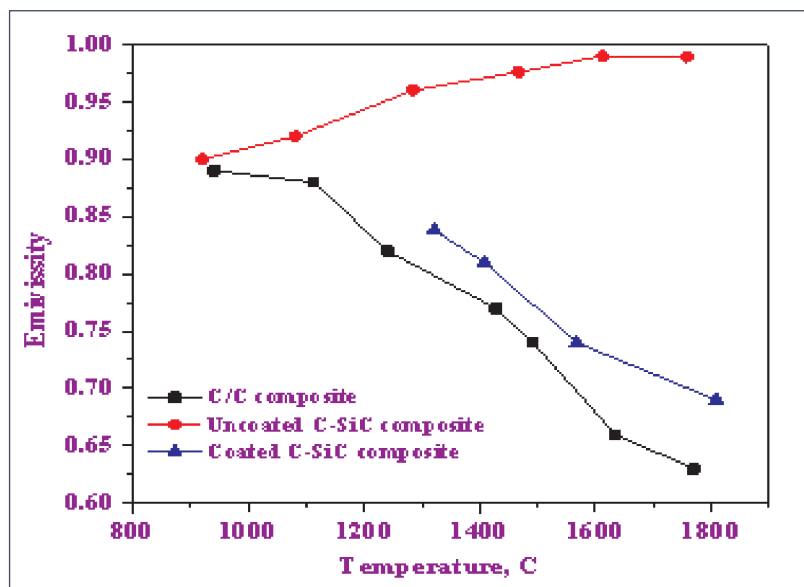
Fig. 16 : Emissivity vs temperature plot of currently used materials for hot structure based thermal protection system in hypersonic vehicle [28]

ZrO$_2$, the amount of which is determined by the composite composition [20]. As a result, the high temperature emissivity of ZrB$_2$-SiC composite will vary depending on the composition.

4.1.3. Catalytic efficiency

Due to the high enthalpy, both oxygen and nitrogen molecules break into atoms as air passes over the bow shock in front of the stagnation point [4]. When oxygen and nitrogen atoms collide on the surface of a heated structure, the material's catalytic support allows them to recombine. The recombination of oxygen and nitrogen atoms into molecules is an exothermic event

that causes strong surface heating. As a result, a lower recombination or catalytic efficiency value is preferable. A few researches on the recombination efficiency of oxygen and nitrogen atoms on ZrB$_2$ and HfB$_2$-based materials have been conducted [6, 29]. Scatteia et al. [29] discovered that the oxygen recombination efficiency on ZrB$_2$-SiC is less than 0.1. With temperature, it follows the Arrhenius characteristic. According to experimental estimates by Marschall et al. [6], the pre exponential coefficient is 5 × 10^{-2}. These experiments are confined to temperatures below 800 ^{0}C. The recombination efficiency of oxygen and nitrogen, on the other hand, might be affected

by the production of oxide scale as a result of oxidation at higher temperatures.

4.2. Properties needed for thermal stress prediction

4.2.1. Elastic modulus and poison ratio

Both the Young's modulus and Poisson's ratio of ZrB_2 and HfB_2 are very high. C11 = 567.8 GPa, C33 = 436.1 GPa, C12 = 56.9 GPa, C13 = 120.5 GPa, and C44 = 247.5 GPa are the experimentally determined elastic constant values of single crystal ZrB_2 [33]. [This gives polycrystalline ZrB_2 Young's modulus and Poisson's ratio of 533 GPa and 0.133, respectively [33]. By first principle calculation, the Young's modulus of polycrystalline ZrB_2 is found to be in the range of 520–550 GPa and the Poisson ratio between 0.137–0.144 [34]. Young's modulus of fully dense hot-pressed monolithic ZrB_2 ranges from 485 to 510 GPa [35]. ZrB_2-SiC composite has a Young's modulus similar to monolithic ZrB_2 [20]. The calculated from 500 GPa of totally dense composite, the Young's modulus of ZrB_2-20 % SiC fell to 456 ± 11 GPa and 401 ± 11 GPa with porosity of 2.2 and 7.3 % [27]. ZrB_2-20 vol% SiC composites with 22.3 %porosity had an elastic modulus of 130 ± 2 GPa. The empirical relationship for the Young's modulus of ZrB_2-SiC is as follows.

$$E=E_0 (1- \alpha P)$$

Where E_0 is the fully dense composite's elastic modulus, P is the porosity, and is constant. With a value of 3.28, the elastic modulus of ZrB_2-20 % SiC composite variation with porosity was found to follow the preceding relationship [27]. At 1300 ^{0}C, the Young's modulus of pure ZrB_2 is maintained at around 70% of ambient temperature [36]. Pure ZrB_2 is claimed to have a rapid reduction in Young's modulus above 1300 ^{0}C. SiC and $MoSi_2$ reinforced ZrB_2 composites exhibit similar characteristics [37-39]. Up to 1500 ^{0}C, ZrB_2- % SiC composite and ZrB_2-20 % $MoSi_2$ composite retain approximately 88% and 75% percent of their room temperature Young's modulus, respectively. Figure 18 shows data from the literature on Young's modulus at high temperatures.

4.2.2. Coefficient of Thermal Expansion (CTE)

Due to rapid aerodynamic heating, the linear coefficient of thermal expansion (CTE) is a significant material parameter for UHTCs, as it determines the amount of strain within the component as well as between surrounding components [4]. The CTE of single crystal ZrB_2 is found to be nearly isotropic, with average values of 6.66×10^{-6} K^{-1} and 6.93×10^{-6} K^{-1} along the a and c-axes, respectively, throughout a temperature range of ambient temperature to 800 ^{0}C [33]. The average CTE for polycrystalline hot pressed ZrB_2 is 6.8×10^{-6} K^{-1} between room temperature and 1000 ^{0}C and 8.4×10^{-6} K^{-1} between 1000 -1400 ^{0}C [24], which is similar to the single crystal
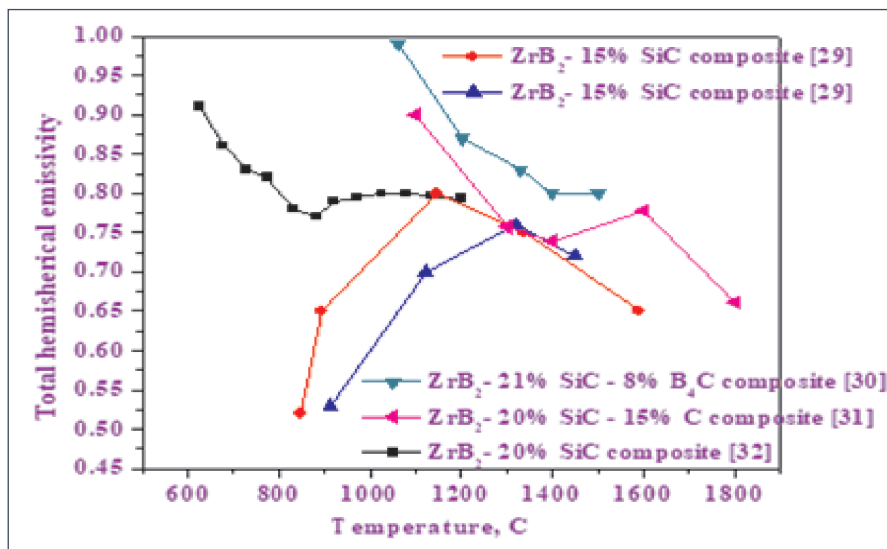
Fig. 17 : Emissivity vs temperature plot of ZrB$_2$-SiC composites
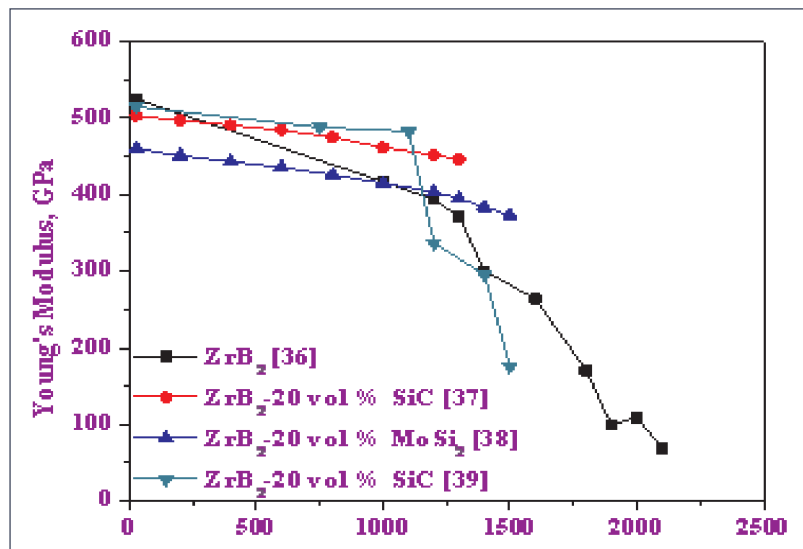
Fig. 18 : Young's modulus of ZrB$_2$ based composites as a function of temperature

value. CTE values of 6.84×10^{-6} K^{-1} and 6.8 × 10^{-6} K^{-1} between room temperature and 1000 ^{0}C have been published for ZrB$_2$ – 20% SiC composites [21] and ZrB$_2$ – 30% SiC composites [24], respectively, whereas CTE of 7.85 × 10^{-6} K^{-1} has been reported for ZrB$_2$ – 20% SiC composite by [22]. However, the CTE value obtained using the rule of mixture and Kerner's model for ZrB$_2$ – 20% SiC is identical to the CTE value published by [21, 24]. Due to compressive residual stress in SiC created while cooling from high temperatures, SiC has no effect on CTE of ZrB$_2$-SiC composites up to 1000 ^{0}C [24]. The CTE value of ZrB$_2$ – 30% SiC composites (7.8× 10^{-6} K^{-1}) is lower than ZrB$_2$ (8.4× 10^{-6} K^{-1}) above 1000 ^{0}C due to SiC's lower CTE (4.5× 10^{-6} K^{-1}) [24]. It demonstrates that residual stress in SiC began to decrease and contribute to expansion, as residual stress in SiC became tensile at 1400 ^{0}C [40].

4.3. Strength

4.3.1. Room temperature

ZrB$_2$ has theoretically computed ideal strengths of 56.9, 53.3, and 41.6 GPa in the 1 2 1 0, 0001, and 10 1 0 directions, respectively [41]. However, the optimum strength of polycrystalline densified ZrB$_2$ is substantially lower. Lu et al. [42] reported strength values of 449 ± 88 MPa and 500 ± 62 MPa for hot pressed monolithic ZrB$_2$ with relative density and grain size of 99 % and 3.9 ± 1.3 μm and

95.1 % and 3± 1 μm, respectively. For pressure-less sintered monolithic ZrB$_2$, Fahrenholtz et al. [43] reported strengths of 489 MPa with relative density and grain size of 94 % and 6 μm, and 370 MPa with relative density and grain size of 100 % and 8 μm. For totally dense monolithic ZrB$_2$ with grain sizes of 3.1± 1.7 μm and 4.1 ± 1.6 μm, Thompson et al. [44] showed better strength for spark plasma sintered sample (460 ± 76 MPa) than hot pressed sample (527± 68 MPa). With grain sizes of 12 – 20 μm, the flexural strength of monolithic ZrB$_2$ with various amounts of B$_4$C is in the range of 320-380 MPa [35].The strength of ZrB$_2$-SiC composites rises with SiC concentration, according to Chamberlain et al. [45] and Zhang et al. [46]. Guo et al. [47] discovered that the strength of ZrB$_2$-SiC composites with 15% SiC is higher than that of composites with 20% SiC. According to Hu and Wang [48], the strength of ZrB$_2$- 15 vol % SiC composites is higher than ZrB$_2$- 30 vol % SiC composites. The strength of ZrB$_2$- SiC composite with 20% SiC is found to be greater than ZrB$_2$-SiC composite with 10% and 30% SiC [20]. The reported strength ratings of ZrB$_2$-SiC composite have a broad range. As high as 1003 ± 94 MPa and as low as 382 ± 24 MPa have been reported. This scatter could be caused by variations in grain size, porosity, processing method, and surface condition of the sample prepared by diamond grinding and electro-discharge machining.
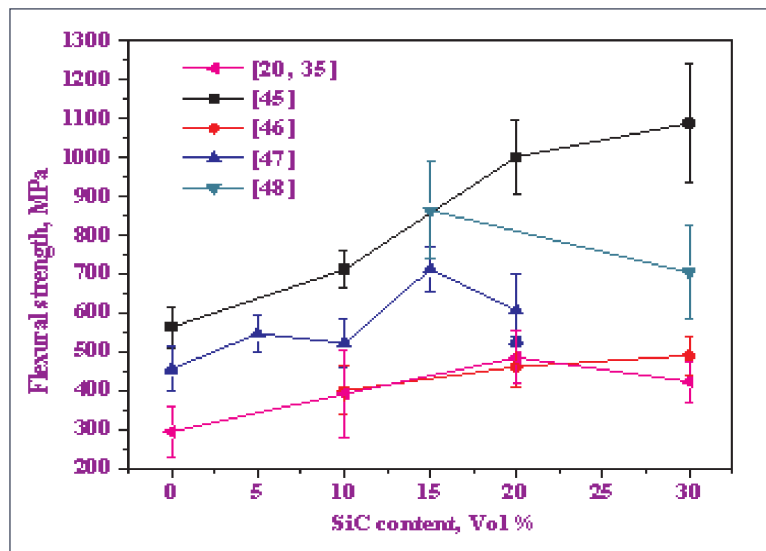
Fig. 19 : The variation of flexural strength of ZrB_2 –SiC composite with SiC contents
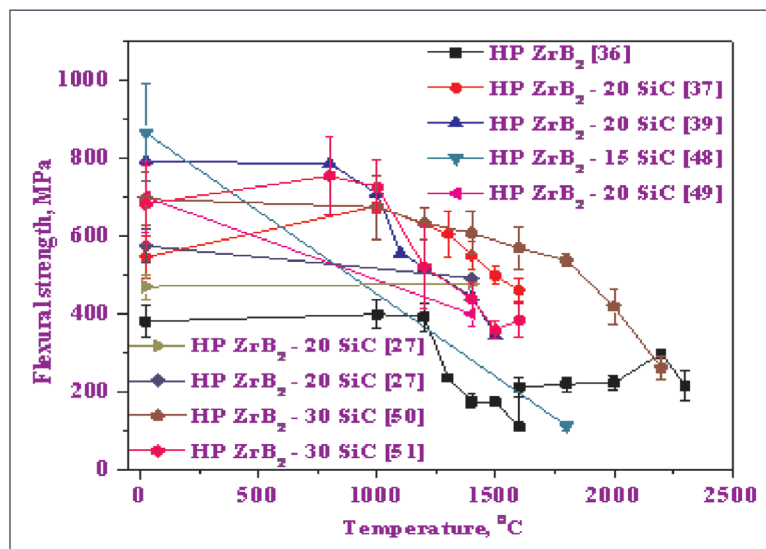
Fig. 20 : Effect of temperature on flexural strength of ZrB_2 and ZrB_2 –SiC composite

4.3.2. High temperature

Figure 20 shows the flexural strength of ZrB_2 and ZrB_2-SiC composites at high temperatures. Up to 1200 ^{0}C, the strength of ZrB_2 does not change considerably, but between 1200 & 1400 ^{0}C, it decreases [36]. Stress reduction by plastic flow is responsible for the drop in strength between 1200 & 1400 ^{0}C [36]. Due to grain boundary softening and grain sliding, the flexural strength of ZrB_2-SiC composite steadily falls at 1000 ^{0}C [37-38]. Data on high temperature strength [27, 36-39, 48-51] reveal that the strength of ZrB_2-SiC composites remained stable up to 1500 ^{0}C

with minor changes. The strength of the ZrB_2-SiC composite rapidly degrades at 1500 ^{0}C. At 1800 ^{0}C, Hu and Wang [48] discovered that the ZrB_2- 15% SiC composite strength had degraded by about 87 % of its room temperature strength. Neuman et al. [51] demonstrated that a ZrB_2- 30% SiC composite retains up to 40% of its strength at 2200 ^{0}C in air. At this temperature, the strength value is important.

4.3.3. Room temperature after exposure at high temperature

During hypersonic flight, a hot structure is exposed to an extreme environment. ZrB_2

and HfB$_2$-based materials are oxidised in this procedure. When these materials are oxidised, they form a multilayer oxide scale on the surface [20]. The number of layers and their content are also affected by the exposure temperature [20]. It is critical to understand the impact of these oxide layer topologies on the strength of these materials for re-usable applications. Figure 21 illustrates the residual flexural strength of hot pressed monolithic ZrB$_2$ and ZrB$_2$-SiC composites after exposure to 1000 ^{0}C, 1500 ^{0}C, and 1700 ^{0}C for 5 hours at room temperature. When compared to unprocessed material, exposure to 1000 ^{0}C increases the strength of monolithic ZrB$_2$ and the ZrB$_2$-SiC composite. Except for ZrB$_2$-10% SiC composite, where the improvement in strength value is about 30% [20, 35], this is a significant improvement in strength values (> 50%) compared to the hot-pressed state. Both monolithic ZrB$_2$ and ZrB$_2$-SiC composite strength values remain unchanged after 5 hours of exposure to 1500 ^{0}C. After 5 hours of exposure to 1700 ^{0}C, the flexural strength of ZrB$_2$-20% SiC and ZrB$_2$-30% SiC composites has significantly decreased. Due to the strength in hot-pressed condition, this was practically degraded to 70%. Hand ZrB$_2$-10% SiC composites, on the other hand, preserved their strength after exposure to 1700 ^{0}C [20]. It is assumed that ZrB$_2$-10% SiC composite is suited for re-usable applications.

4.3.4. Performance evaluation of ZrB$_2$ and HfB$_2$ as sharp hot structure

HfB$_2$ and ZrB$_2$-based materials are evaluated for their performance as sharp hot structures using arc jet testing or inductively coupled plasma (ICP) wind tunnels for various capacities under NASA Sharp Hypersonic Aero-thermodynamic Research [4] and European programme ATLLAS (Aerodynamic and Thermal Load Interactions with Lightweight Advanced Materials for High Speed Flight) [52]. In approximately 60 seconds, a hemispherical arc jet sample of ZrB$_2$-SiC composite with a 7.5 mm radius of curvature achieved 1850 ^{0}C and reached 1930 ^{0}C with a specific enthalpy of 20 MJ/kg [53]. Figure 22 depicts a complete surface temperature profile as well as the sample appearance following arc jet testing a ZrB$_2$-SiC composite sample. Zhang et al. [54] discovered that ZrB$_2$-SiC composite is a superior prospective material for sharp hot structures than the C$_f$-SiC composite currently in use in a simulated re-entry scenario. Figure 23 exhibits micrographs of C$_f$-SiC composite and ZrB$_2$-SiC composite arc jet-tested samples with 3.5 mm radius of curvature. After 100 s of irradiation, significant degradation was seen in the C$_f$-SiC composite [54]. After 200 s of exposure, however, no cracks are discovered in the ZrB$_2$-SiC composite [54]. This demonstrates that ZrB$_2$-SiC composite is superior to C$_f$-SiC composite. Parthasarathy
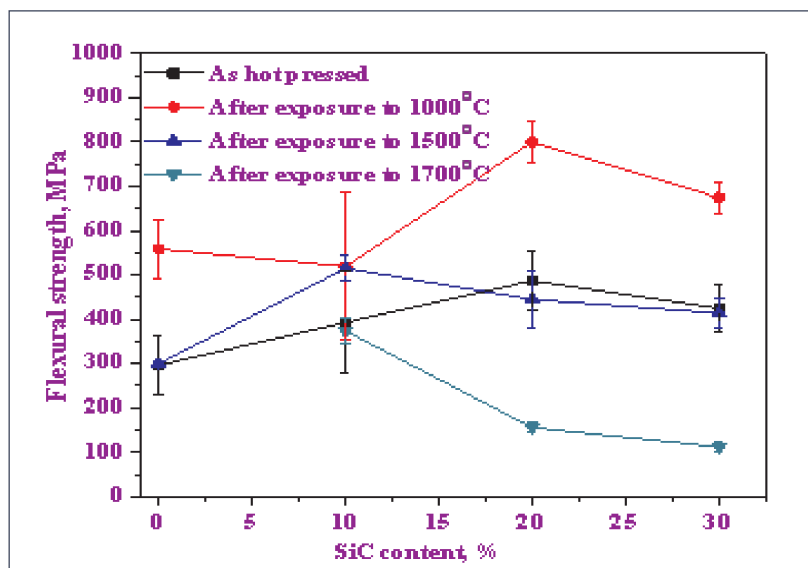
Fig. 21 : Effect of high temperature exposure on flexural strength of monolithic ZrB$_2$ and ZrB$_2$- SiC composite [20, 35]

et al. [55] found that HfB$_2$-SiC composite samples outlasted sintered SiC samples in a similar experiment. Under conditions simulating free flight at a height of 25 km at Mach 6.25, HfB$_2$-SiC composite samples can withstand exposures of up to 900 s, and up to 80 s at Mach 7 [55].
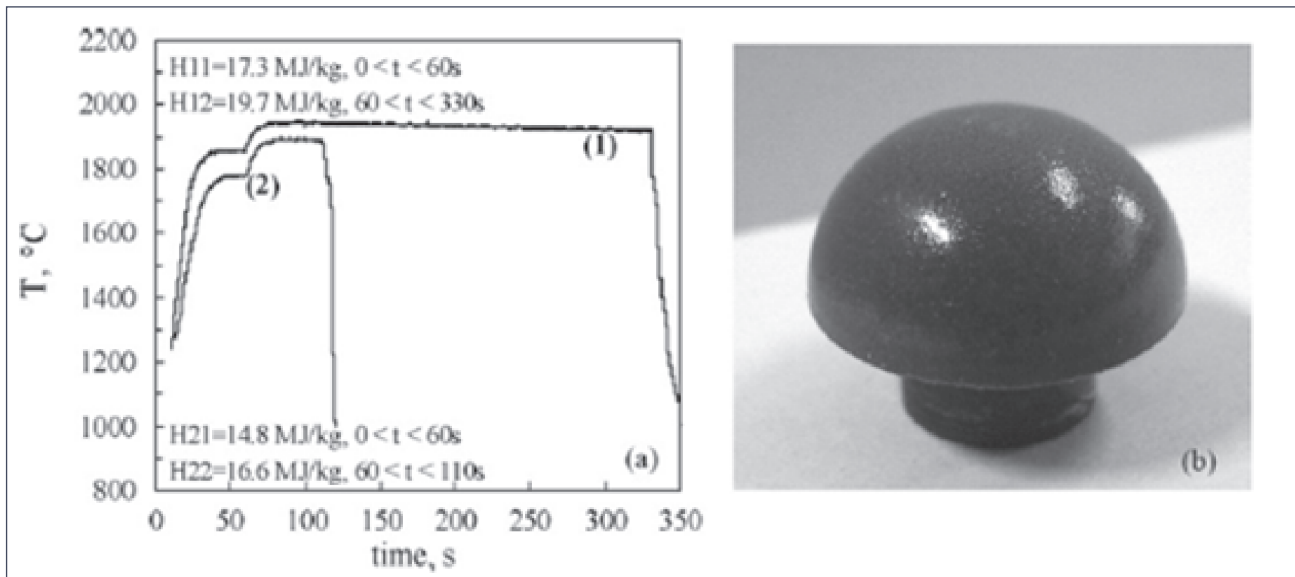
Fig. 22 : (a) A surface temperature profile for ZrB$_2$-SiC composite under arc jet testing under total enthalpy of 10-20 MJ/Kg (equivalent to 800 -1000 W/cm^2), (b) the appearance of ZrB$_2$-SiC composite after experiencing 1930 ^{0}C under arc jet testing [53]
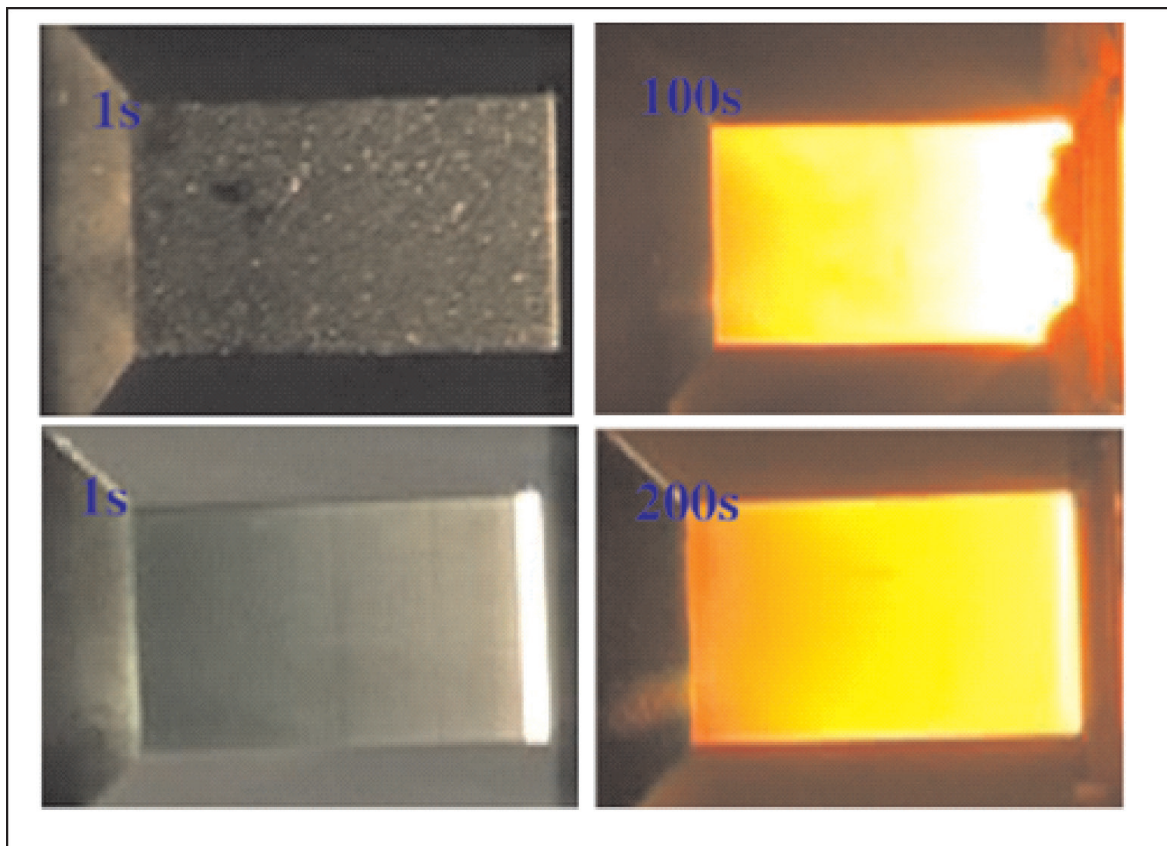
Fig. 23 : Test specimen after arc jet testing, the surface temperature ~ 1450 ^{0}C [54]

5. Summary

Sharp hot structures in hypersonic vehicles could be made of ZrB_2 and HfB_2 reinforced with Si-based materials (such as SiC and $MoSi_2$). The hot structure (a passive thermal protection system) can act as a semi-cooled structure due to the high thermal conductivity of ZrB_2 and HfB_2-based materials at very high temperatures. As ZrB_2 and HfB_2-based materials have excellent strength retention at high temperatures, they can withstand thermal and aerodynamic stress. At high temperatures, oxidation of ZrB_2 and HfB_2-based materials changes their characteristics. As a result, in order to acquire a fair estimate of surface temperature and thermal stress, the component designer must consider the effect of oxidation on fundamental properties of these materials.

References

[1] J. J. Bertin and R. M. Cummings, "Fifty years of hypersonics: where we've been, where we're going," Progress in Aerospace Sciences 39 (2003) 511–536

[2] D. M. V. Wie, S. M. D'Alessio and M. E. White, "Hypersonic Airbreathing Propulsion," Johns Hopkins APL Technical Digest, Volume 26, N umber 4 (2005)

[3] D. E. Glass, "Ceramic Matrix Composite (CMC) Thermal Protection Systems (TPS) and Hot Structures for Hypersonic Vehicles," 15th AIAA Space Planes and Hypersonic Systems and Technologies Conference, AIAA-2008-2682

[4] T. H. Squire and J. Marschall, "Material property requirements for analysis and design of UHTC components in hypersonic applications," J. Euro. Ceram. Soc., 30 (2010) 2239–2251

[5] R. Savino, R. M. De S. Fumo, D. Paterna, A. D. Maso and F. Monteverde, "Arc-jet testing of ultra-high-temperature-ceramics," Aerospace Science and Technology, 14 (2010) 178–187

[6] J.Marschall, A. Chamberlain, D. Crunkleton and B. Rogers, "Catalytic atom recombination on ZrB2/SiC and HfB2/SiCultra high temperature ceramic composites," J. Spacecrafts and Rockets, 41 (2004) 576-581

[7] J.Marschall and D. G. Fletcher, "High-enthalpy test environments, flow modeling and in situ diagnostics for characterizing ultra-high temperature ceramics," J. Euro. Ceram. Soc., 30 (2010) 2323-2336

[8] T. A. Parthasarathy, M. D. Petry, G. Jefferson, M. K. Cinibulk, T. Mathur and M. R. Gruber, "Development of a Test to Evaluate Aerothermal Response of Materials to Hypersonic Flow Using a Scramjet Wind Tunnel," Int. J. Appl. Ceram. Technol., 8 (2011) 832–847

[9] D. M. Van Wie, D. G. Drewry Jr., D. E. King, C. M. Hudson, "The hypersonic environment: Required operating conditions and design challenges," J. Mater. Sci., 39 (2004) 5915 – 5924

[10] W. F. N. Santos, "Leading edge bluntness effects on aerodynamic heating and drag of power law body in low-density hypersonic flow," ABCM, 26 (200) 5236-243

[11] M. Patel, PhD Thesis, "Densification, oxidation, mechanical and thermal behaviour of zirconium diboride (ZrB2) and zirconium diboride – silicon carbide (ZrB2-SiC) composites," Indian Institute of Science, Bangalore, India, 2014

[12] S. P. Walker and B. J. Sullivan, "Sharp refractory composite leading edges on hypersonic vehicles," American Institute of Aeronautics and Astronautics, 1-9 (2003)

[13] M.M. Opeka, I. G. Talmy and J. A. Zaykoski "Oxidation-based materials selection for 2000 0C + hypersonic aerosurfaces: Theoretical considerations and historical experience," J. Mater. Sci., 39 (2004) 5887 – 04

[14] E. Wuchina, E. Opila, M. Opeka, W. Fahrenholtz, and I. Talmy, "UHTCs: Ultra-high temperature ceramic materials for extreme environment applications," Interface, (2007) 30-36.

[15] K. Upadhya, J. M. Yang, and W. P. Hoffman, "Materials for ultrahigh temperature structural applications," American ceramic society bulletin, 76 (1997) 51– 56

[16] C. W. Ohlhorst, "Thermal conductivity database of various structural carbon- carbon composite materials," NASA Technical Memorandum 4787 (1997)

[17] Ceramic matrix composite: fibre reinforced ceramics and their application, edited by W. Krenkel, WILEY-WCH, 2008

[18] H. Kinoshita, S. Otani, S. Kamiyama, H. Amano, I. Akasaki, J. Suda, Zirconium diboride (0 0 0 1) as an electrically conductive lattice matched substrate for gallium nitride. Jpn J Appl Phys 40 (2001) L1280

[19] M. Patel, V.V. B. Prasad, V. Jayaram, "Heat conduction mechanisms in hot pressed ZrB2 and ZrB2–SiC composites," J. Eur. Ceram. Soc.," 33 (2013) 1615–1624

[20] M. Patel, J. J. Reddy, V.V. B. Prasad, V. Jayaram, "Strength of hot pressed ZrB2–SiC composite after exposure to high temperatures (1000–1700 0C)," J. Eur. Ceram. Soc., 32 (2012) 4455-4467

[21] R. Loehman, E. Corral, H. P. Dumm, P. Kotula, R. Tandon, "Ultra-high temperature ceramics for hypersonic vehicle applications," Sandia Report, SAND2006-2925. Albuquerque, NM; June 2006

[22] M. Mallik, A. J. Kailath, K. K Ray, R. Mitra, "Electrical and thermophysical properties of ZrB2 and HfB2 based composites," J Eur Ceram Soc, 32 (2012) 2545–55

[23] L. Zhang, D. A. Pejakovič̌c, J. Marschall, M. Gasch,"Thermal and electrical transport properties of spark plasma-sintered HfB2 and ZrB2 ceramics," J Am Ceram Soc,94 (2011) 2562–70

[24] J. W. Zimmermann, G. E. Hilmas, W. G. Fahrenholtz, R. B. Dinwiddie, W. D. Porter, H. Wang, "Thermophysical properties of ZrB2 and ZrB2–SiC ceramics," J Am Ceram Soc, 91 (2008) 1405–11

[25] M. Gasch, S. Johnson, J. Marschall, "Thermal conductivity characterization of hafnium diboride-based ultra high temperature ceramics," J Am Ceram Soc, 91(2008) 1423–32

[26] M. Gasch, D. Ellerby, E. Irby, S. Beckman, M. Gusman, S. Johnson, Processing, properties and arc jet oxidation of hafnium diboride/silicon carbide ultra high temperature ceramics, J. Mater. Sci. 39 (2004) 5925 – 5937

[27] M. Patel, V.V. B. Prasad, unpublished work, 2014

[28] C. W. Ohlhorst, W. L. Vaughn, K. Daryabeigi, R. K. Lewis, A. C. Rodriguez, J. D. Milhoan, J. R. Koenig, "Emissivity Results On High Temperature Coatings for Refractory Composite Materials," J Eur Ceram Soc, 34 (2014) 1-11

[29] L. Scatteia, D. Alfano, F. Monteverde J. L. Sans, M. B. Pichelin, Effect of the Machining Method on the Catalycity and Emissivity of ZrB2and ZrB2–HfB2-Based Ceramics, J. Am. Ceram. Soc., 91 (2008) 1461–1468

[30] G V. Laningham, Y. Berta and R. F. Speyer, "Spectral emittance of resistively heated oxidized ZrB2-30 mol% SiC," J. Mater. Res., 27 (2012) 2520-2527

[31] S. Meng, H. Chen, J. Hu, Z. Wang, " Radiative properties characterization of ZrB2-SiC based ultra high temperature ceramic at high temperature," Mater. Design, 21 (2011) 377-381

[32] W. Tan, C. A. Petorak, R. W. Trice, "Rare-earth modified zirconium diboride high emissivity coatings for hypersonic applications," J Eur Ceram Soc, (2013)

[33] N. L. Okamoto, M. Kusakari, K. Tanaka, H. Inui, S. Otani, "Temperature dependence of thermal expansion and elastic constants of single crystals of ZrB2 and the suitability of ZrB2 as a substrate for GaN film," J. Appl. Phy., 93 (2003) 88-93

[34] X. Zhang, X. Luo, J. Han, J. Li, W. Han, "Electronic structure, elasticity and hardness of diborides of zirconium and hafnium: First principles calculations," Comp. Mater. Sci., 44 (2008) 411–421

[35] M. Patel, J.J. Reddy, V.V. B. Prasad, J. Subrahmanyam, V. Jayaram, "Residual strength of hot pressed zirconium diboride (ZrB2) after exposure to high Temperatures," Mater. Sci. Engg. A 535, 189– 196 (2012)

[36] E. W. Neuman, G. E. Hilmas, W. G. Fahrenholtz, Strength of zirconium diboride to 2300°C, J. Am. Ceram. Soc., 1–4 (2012)

[37] J. Zou,G. J. Zhang, C. F. Hu, T. Nishimura, Y. Sakka, H. Tanaka, J. Vleugels, O. V. Biest, High temperature bending strength, internal friction and stiffness of ZrB2–20 vol% SiC ceramics, J. Euro. Ceram. Soc, 32 (2012) 2519–2527

[38] S. Guicciardi, A. K. Swarnakar, O. V. Biest and D. Sciti, "Temperature dependence of the dynamic Young's modulus of ZrB2–MoSi2 ultra-refractory ceramic composites," Scripta Mater., 62 (2010) 831–834

[39] M. W. Bird, R. P. Aune, A. F. Thomas, P. F. Becher, K. W. White, Temperature-dependent mechanical and long crack behavior of zirconium diboride–silicon carbide composite, J. Euro. Ceram. Soc., 32 (2012) 3453–62

[40] J. Watts, G. E. Hilmas, W. G. Fahrenholtz, "Mechanical Characterization of ZrB2–SiC Composites with Varying SiC Particle Sizes", J. Am. Ceram. Soc., 94 (2011) 4410–4418

[41] X. Zhang, X. Luo, J. Li, P. Hu and J. Han "The ideal strength of transition metal diborides TMB2 (TM = Ti, Zr, Hf): Plastic anisotropy and the role of prismatic slip,"Scripta Mater., 62 (2010) 625–628

[42] Z. Lu, D. Jiang, J. Zhang, Q. Lin, "Microstructure and mechanical properties of zirconium diboride obtained by aqueous tape casting process and hot pressing. J Am Cerom Soc, 93 (2010) 4153–4157

[43] W. G. Fahrenholtz, G. E. Hilmas, S. C. Zhang, S. Zhu, "Pressureless sintering of zirconium diboride: Particle size and additive effects," J Am Cerom Soc., 91 (2008)1398–1404

[44] M. Thompson,W. G. Fahrenholtz, G. E. Hilmas, "Effect of starting particle size and oxygen content on densification of ZrB2," J Am Cerom Soc.,94 (2011) 429-435

[45] A. L. Chamberlain, W. G. Fahrenholtz, G. E. Hilmas, "High-strength zirconium diboride-based ceramics," J Am CeromSoc, 87(2004) 1170–1172

[46] S. C. Zhang, W. G. Fahrenholtz, G. E. Hilmas, "Mechanical properties of sintered ZrB2–SiC ceramics," J. Euro. Ceram. Soc., 31 (2011) 893-901

[47] S. Q. Guo, J. M. Yang, H. Tanaka and Y. Kagawa, "Effect of thermal exposure on strength of ZrB2-based composites with nano-sized SiC particles," Comp. Sci. Tech., 68 (2008) 3033–3040

[48] P. Hu and Z. Wang, "Flexural strength and fracture behavior of ZrB2–SiC ultra-high temperature ceramic composites at 1800C," J. Euro. Ceram. Soc., 30 (2010) 1021–1026

[49] E. Z. Solvas, D. D. Jayaseelan, H. T. Lin, P. Brown, W.E. Lee "Mechanical properties of ZrB2- and HfB2- based ultra-high temperature ceramics fabricated by spark plasma sintering," J. Euro. Ceram. Soc., 33 (2013) 1373-1386

[50] E. W. Neuman, G. E. Hilmas, W. G. Fahrenholtz, "Mechanical behavior of zirconium-silicon carbide –boron carbide ceramics up to 2200 0C, J. Euro. Ceram. Soc., 35 (2015) 463-476

[51] E. W. Neuman, G. E. Hilmas, W. G. Fahrenholtz, "Mechanical behavior of zirconium-silicon carbide ceramics at elevated temperature in air," J. Euro. Ceram. Soc., 33 (2013) 2889-99

[52] J. F. Justin and A. Jankowiak, "Ultra High Temperature Ceramics: Densification, Properties and Thermal Stability," The Dnera journal of aerospace lab, 3 (2011) 1-11

[53] F. Monteverde and R. Savino, "Stability of ultra-high-temperature ZrB2–SiC ceramics under simulated atmospheric re-entry conditions," J. Euro. Ceram. Soc., 27 (2007) 4797–4805

[54] X. Zhang,P. Hu, J. Han, S. Meng, "Ablation behavior of ZrB2–SiC ultra high temperature ceramics under simulated atmospheric re-entry conditions," Comp. Sci. Tech., 68 (2008) 1718–1726

[55] T. A. Parthasarathy, M. D. Petry, M. K. Cinibulk, T. Mathur and M. R. Gruber, "Thermal and Oxidation Response of UHTC Leading Edge Samples Exposed to Simulated Hypersonic Flight Conditions," J Am CeromSoc, 96(2013) 907–915

****

A Simpler Approach to Molecule Based Magnetism: Tweaking the Role of Ligands

Joy Chakraborty*, Rakesh K Gupta, Suresh Kumar and N Eswara Prasad

Abstract

The race towards miniaturization is one of the most challenging and fascinating fields for today's scientific and technological community. Much of the knowledge in classical chemistry has been directed into the design and synthesis of systems that can mimic various kinds of devices at the molecular and supra-molecular scale. Hence the chemistry of paramagnetic poly-nuclear transition metal complexes has been motivating chemists who are studying the molecular magnetism to discover new paramagnetic systems at the molecular levels. The synthetic strategies employed to prepare such systems have varied from the combination of paramagnetic metal ions with flexible organic ligands/radicals that bridge between the metals in a fashion which may lead to a high ground state spin molecule. Advantages of these materials are manifold due to the following reasons: (i) they exhibit the same phenomenon at molecular level purity, (ii) they show high thermal and chemical stability, (iii) easier synthesis, (iv) highly reproducible properties, (v) rich synthetic behaviour allowing functionalization of the peripheral organic ligands, (vi) high processability and (vii) low cost. In this report, we will try to explore the role of various novel Schiff-base ligands and their specific bridging modes in exploring the magnetic behaviour of a few multinuclear/supra-molecular clusters.

Keywords: Molecule based magnetism; Transition metals; Schiff-base; Bridging ligands; Magnetic pathways.

1. Molecule-based Magnets : Introduction and General Overview

As we know that the push up limits of silicon are approached day by day, the likelihood of 'engineering up' from a targeted molecule to functional electronic devices offers the most promising alternative route to the design of materials for viable use in the molecular scale and beyond. The principal aim is to plan and assemble molecular level devices that may not only reduce dimensions and but also increase speed by several orders of magnitude. Hence, scientists are targeting such molecular systems which are easily switchable between two available spin states. Therefore, molecule-based magnetism is nowadays considered a rapidly developing field [1-2]. Recently, spectacular advances have been made in the development and implementation of nano-sized magnetic materials in information storage where they can easily reverse their magnetic moments when exposed to external magnetic field and are already widely in use [3].

Thus, molecular magnetism is a multidisciplinary area which conjugates synthesis of molecules having specific magnetic properties and theoretical analysis aimed at mechanistic consideration of the relation of these properties with the electronic structure. It can be supra-molecular in nature, since it results from the collective features of components bearing free spins and on their specific magnetic pathway in organised assemblies. Hence, the engineering of molecular magnetic systems requires the search for suitable paramagnetic metal ions and their

arrangement in suitable multinuclear cluster or supra-molecular architectures which may enable spin coupling and alignment. Hence the main challenge for a chemist in the design of molecular magnets is controlling the molecular topology to obtain interactions between spin carriers in three-dimensional network involving a specific type of building block.

There innovative organometallic and increasingly coordination chemistry come into picture as the centre of development in such molecule-based magnets. Intuitive ligand design is essential for implementing controlled modifications to the electronic structure and magnetic properties of d and f-block transition metal clusters. Rational use of non-traditional ligands based on low-coordinate main group elements also drive the field forward. In this report, molecular magnetism has been seen from the perspective of ligands, especially novel Schiff-bases and their bridging properties, in achieving the same. Due emphasis has been placed on the role played by such novel ligands in bridging magnetic pathways between transition metal/f-element centres. Such non-traditional ligands, with their relatively diffuse valence orbitals and more diverse bonding characteristics, also present scope for fine tuning the spin-orbit coupling properties and metal-ligand covalency in such molecular magnets, which has implications in areas such as spin-crossover phenomena and magnetic exchange coupling. The chemistry of such clusters encompasses vast areas of d-block transition metals, f-block lanthanides based multinuclear clusters, as defining the state of the art.

2. Cooperative Magnetism and Role of Ligands on Exchange Pathways

The particular beauty and fascinating diversity of the structures which can be obtained by assembling metal ions and various multifunctional ligands, has attracted the chemists to explore the field of crystal design and engineering of poly-dimensional arrays and networks containing the metal ions. In this regard it deserves special mention that generally two components are necessary in every synthetic approach leading to extended supra-molecular multi-nuclear assemblies: the ligand or spacer (organic tecton) and the proper choice of metal ions suitable to build a particular assembly. From the perspective of crystal engineering, the benefit of using transition and inner transition metal ions is that the shape of the coordination building unit can be controlled by choosing the coordination geometries of the metal ions properly. In the language of supra-molecular chemistry, the ligand is a programmed species, whose information is read by the metal ions according to their coordination algorithm. Thus, a more specific geometry can be obtained by the judicious attachment of suitable functional substituents to the ligands, which will act as intra- and/or intermolecular connectors. The main aspect that is especially relevant for such studies stems from the understanding of the fundamental science of magnetism and magneto-structural correlations in complex molecular systems. Among the various bridging ligands, carbonato-, chloro-, oxo-, phenoxo-, dicyanamido, cyano-, azido-, pyrazine, 4,4'-bipyridyl, acetato- etc. have drawn considerable attention due to their widespread applications in various fields such as (i) molecular magnetism, (ii) photochemical activity, (iii) intervalence electron transfer etc. Out of them, the most stimulating area of interest is the synthesis of multi- or poly-nuclear coordination complexes with interesting magnetic properties which has undergone spectacular advances in the last decade. They can show different magnetic phenomenon i.e. (i) dia-magnetism, (ii) super-diamagnetism, (iii) paramagnetism, (iv) super-paramagnetism, (v) ferromagnetism, (vi) anti-ferromagnetism, (vii) ferrimagnetism, (viii) meta-magnetism to (ix) spin-glass.

Materials are classified as diamagnetic when they like to be repelled by a magnetic field and paramagnetic when they tend to move into the magnetic field. Paramagnetism stems from the presence of one or more unpaired electron spin which is totally absent in a diamagnetic substance. In a free atom or ion, both the orbital and the spin angular momenta give rise to a net magnetic moment. But when the same atom or ion is part of a complex, its orbital angular momentum can be eliminated (quenched) – as

a result of the interactions of the electrons with their environment. Quenching is more important for d-electrons than for f-electrons, which are deeply buried in atoms and often experience their environment only weakly. Hence, whereas d-block metal complexes are more pronounced from magnetic point of view despite the quenching phenomena, it is not generally true for f-block complexes. Diamagnetism and paramagnetism are specially the characteristic of individual atoms and complexes, whereas properties such as ferromagnetism, anti-ferromagnetism or ferrimagnetism depend on interactions between electron spins on many atoms and arise from the cooperative behaviour of many unit cells in a crystal. These two are significant instances of the Cooperative magnetism.

In a ferromagnetic substance, the spins on different metal centres are coupled into a parallel alignment that is sustained over thousands of atoms in a magnetic domain [Fig. 1(a)]. Since the magnetic moments of individual spins augment each other, the net magnetic moment may become very large. Moreover, once established and the temperature maintained below the Curie temperature (T_c), the magnetization persists since the spins are locked together. The key feature is that this interaction is strong enough to align the spin vectors but not that much strong to form covalent bonds, where the electrons are paired. Furthermore, a hysteresis loop is observed. The loop is broad for hard ferromagnets while it is narrower for soft ferromagnets.

In an anti-ferromagnetic substance, neighbouring spins are locked into an anti-parallel alignment and the complex may show a low magnetic moment [Fig. 1(b)]. Anti-ferromagnetism is often observed when a paramagnetic substance is cooled gradually to a low temperature and is signalled by a decrease in magnetic susceptibility with decreasing temperature. The critical temperature for the onset of anti-ferromagnetism is called the Néel temperature (T_N). The spin coupling responsible for anti-ferromagnetism usually occurs via the intervening ligands. The spin on one metal atom induces a small spin polarisation on an occupied orbital of a ligand and these result in alignment of spin on adjacent metal atom that is antiparallel to the first [Fig. 1(c)]. Coupling of spins through the intervening ligands is frequently observed in molecular complexes containing two ligand-bridged metal ions.

Unlike conventional organic-free magnets used in human society since the 12th century, the organic species of molecule-based magnets exhibit a wide variety of bonding and structural motifs. These include isolated molecules (zero dimensional - 0D), and those with extended bonding within chains (1D), within layers (2D), and within 3D network structures. A further classification into subgroups is performed according to the exhibited type of magnetic ordering like: meta-magnetism, canted anti-ferromagnetism, spin-glass behaviour. The magnetic exchange interactions between the paramagnetic transition metal ions in bi-nuclear

(a)　　　　　(b)　　　　　(c)
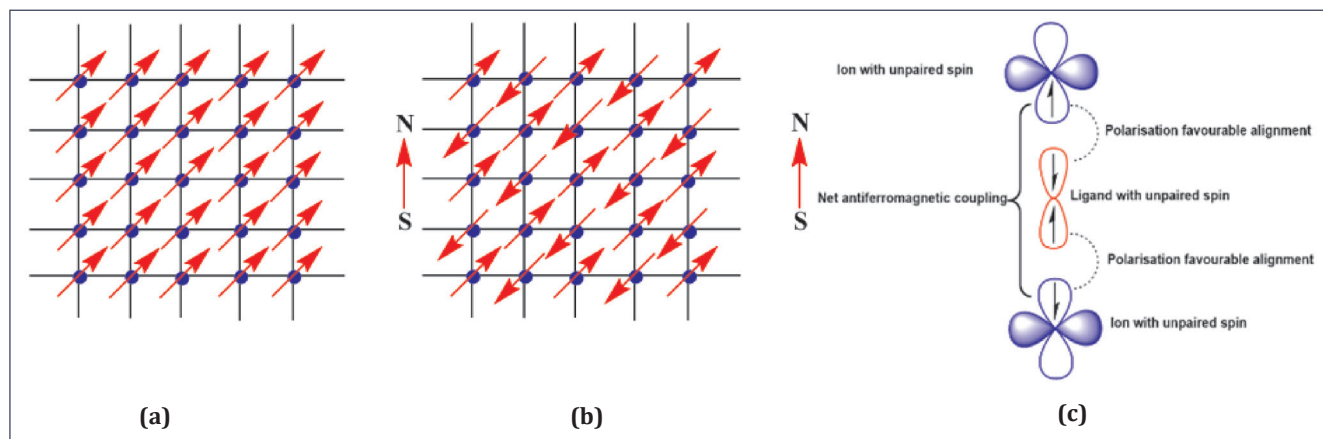
Fig. 1 : (a) Spin alignment in ferromagnetic materials; (b) Spin alignment in antiferromagnetic materials; (c) Spin polarisation

and poly-nuclear transition metal complexes are ideally suitable for the study of intra-molecular magnetic exchange interactions, where the transition metal ions are the magnetic moment carrier. These interactions may arise from the direct overlapping of magnetic orbitals of two connected metal centres or via super-exchange through the bridging atoms like O, N, S etc. Such interactions may either increase or decrease the magnetic moment of the complex as a whole thereby guiding the nature of magnetism to be exhibited by the system. Chemists are therefore interested in the molecular design and synthesis of simple magnetic systems/molecule-based magnetic materials. Extensive research is going on for increasing the structural and magnetic complexity of the systems so that it is possible to control the passage from molecular assemblies to functional magnetic materials.

3. A Brief Discussion on General Synthesis Methodology

Schiff-bases, originally known by the name of Hugo Schiff, are aldehyde and ketone-like compounds in which the carbonyl functional group is substituted by either imine or azomethine group. They are formed when any primary amine group reacts with carbonyl under specific conditions. Hence structurally it is nitrogen analogue of a carbonyl group. Schiff-base macrocycles have been of great importance in both organic and inorganic chemistry. They were among the first artificial metal complexes to be synthesized.

A Schiff-base chelator ligand can be prepared as per following example [Fig. 2]. Benzhydrazide (source of primary amine functionality) is refluxed with 2-hydroxy-3-methoxybenzaldehyde (source of ketone functionality) in super dry methanol [4]. After 6 hours of continuous reflux at 80 °C, a deep yellow solution is obtained. Drastic change in color from colorless to deep yellow suggests the formation of Schiff base with imine functional group (in this particular case (E)-N'-(2-hydroxy-3-methoxybenzylidene) benzohydrazide). It is further subjected to TLC, to reveal the presence of some unreacted starting materials along with the Schiff-base product. The Schiff-base ligand is isolated by column chromatography in order to get in purified form. The purified solution is then evaporated to get fine crystalline product of the Schiff-base ligand. It is dried and stored in vacuo over $CaCl_2$ for subsequent use. The purity of the product may be ascertained by UV-Vis, NMR, FT-IR, ESI-MS, TGA, DSC and CHNSO analyses.

The metal cluster complexes can be synthesized in the following way. The appropriate quantity of solid pure Schiff-base ligand is dissolved in super dry methanol or any other appropriate solvent. A solution of metal perchlorate/nitrate/chloride is prepared in suitable super dry solvent. Then the ligand solution is added drop by drop to the metal salt solution. Other linear or bridging linker ligands like azide, cyanate, thiocyanate solution may be added at appropriate molar ratio. The mixture is stirred and refluxed for 3 hours. The resulting solution is then filtered off and the filtrate is left undisturbed. Single crystals of X-ray diffraction quality are prepared. They are filtered and dried over $CaCl_2$. The purity of the product may be ascertained by single crystal XRD, UV-Vis, NMR, FT-IR, ESI-MS, TGA, DSC and CHNSO analyses.
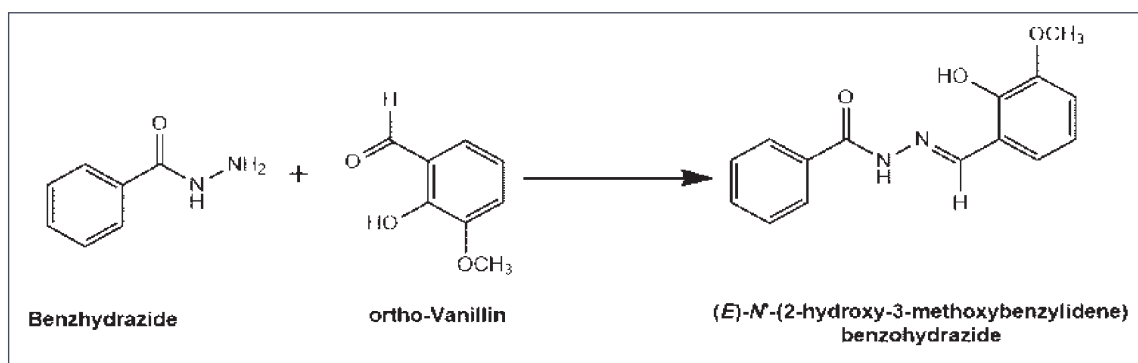

Fig. 2: Representative example of Schiff base ligand synthesis

4. Tweaking the Role of Ligands in Achieving Magnetic Coupling

With the aim of continuing the magnetochemistry study of poly-nuclear complexes, considerable effort have been given to prepare the Cu(II) complexes with potentially multi-dentate Schiff-base ligand for example (E)-N'-(2-hydroxy-3-methoxybenzylidene) benzohydrazide.

Utilisation of such poly-dentate Schiff- base ligands is very much important as they can function with both bridging and chelating capacities and represent a promising route to the synthesis of innovative spin clusters. When the ligand coordinates with Cu(II) in 1:1 molar ratio, the coordination sphere of the Cu(II) ion remains unsaturated. Therefore, the complex has a tendency to polymerize, giving multi-nuclear complexes or to further coordinate with additional ligands, forming novel 1:1 (M:L) complexes showing enhanced nuclearity like in this example of a novel tetra(μ_3-phenoxo) bridged tetranuclear cubane core Cu(II) complex. The Cu_4O_4 cubane core consists of four μ_3-phenoxo-bridged copper(II) atoms giving an approximately cubic array of alternating copper(II) and oxygen atoms [Fig. 3(a)]. Cryomagnetic susceptibility measurements over a wide range of temperature (2–300 K) under 0.5 T magnetic field reveals both ferromagnetic and antiferromagnetic interactions in a 2J model [J_{11} = +13.6(4) cm^{-1} and J_{12} = -34.9(4) cm^{-1} which in turn results in an overall anti-ferromagnetic behaviour of the magnetic system [Fig. 3(b)].

Another prominent example is of one End-to-End di-azido bridged Cu(II) multi-nuclear complex [Fig. 4(a)]. End-on (EO) dibridged azido complexes are well known in the literature and magneto-structural correlations have determined that the coupling is ferromagnetic for bridging Cu–N–Cu angles <108^0 [5]. In end-to-end (EE) dibridged azido complexes with Cu(II) exhibiting its common elongated octahedral or square pyramidal coordination geometry in its 6 or 5 coordination environment, the EE linkage can occur via two different routes: in the equatorial–equatorial configuration, where the azido group coordinates via the equatorial bonds to both the copper atoms, strong anti-ferromagnetic coupling can occur since the σ orbitals on the azido group couple directly with the unpaired electron density in the d_{x2-y2} orbitals. In contrast, if the bridging conformation involves an equatorial linkage to one of the Cu ions and an axial linkage to the second (equatorial–axial), the coupling is expected to be a weak one, since there is a little
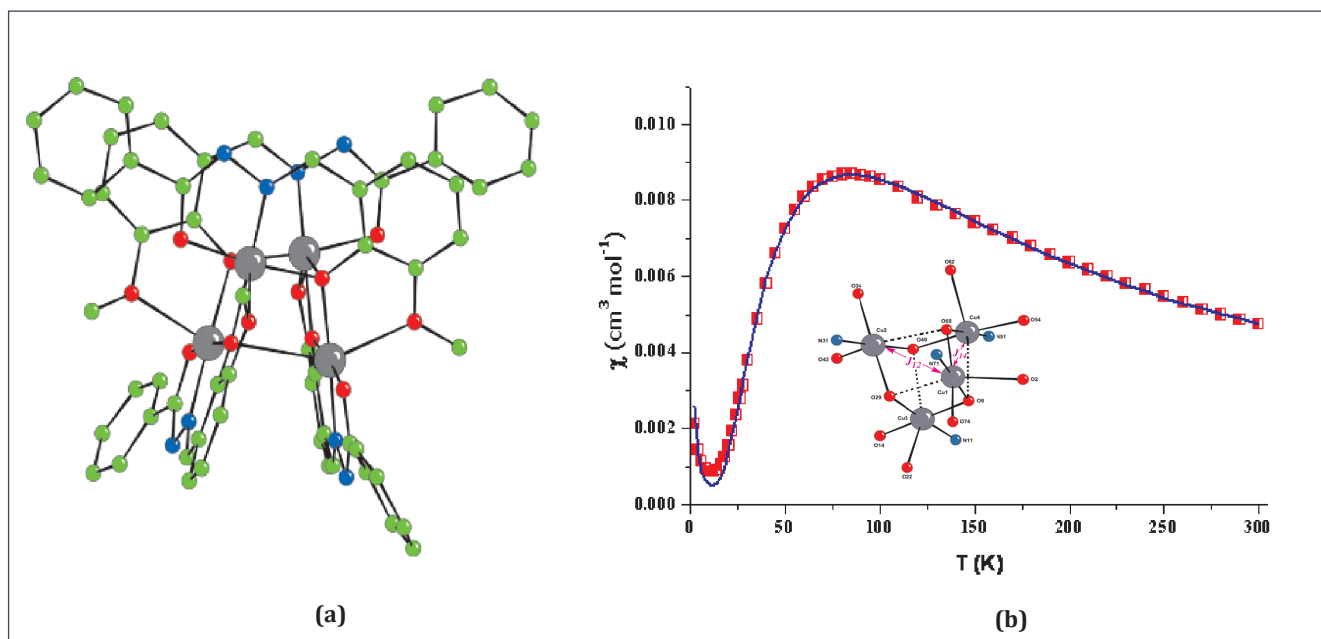

(a)

(b)

Fig. 3 : (a) tetra(μ_3-phenoxo) bridged tetranuclear Cu(II) complex; (b) Temperature dependence of magnetic susceptibility, (Inset) Magnetic exchange pathways in Cu_4O_4 cubane core

overlap of the azido σ and π orbitals with the magnetic d_{x2-y2} orbital via the axial interaction. The magnetic behaviour of the complex is shown in Fig. 4(b). The shape of this curve indicates dominant ferromagnetic coupling until 9.5 K, which results from the interaction of the copper(II) ions through the double end-to-end azide bridge [Fig. 4(b)].

Similarly, extensive research effort for the last 25 years has been focused on the design, template synthesis and characterization of the new polyaza and polyoxaaza Schiff-base homo- or heterodinuclear complexes of metal ions of varying radii and electron configuration [6-9], which are of significant importance in terms of magnetic properties. Schiff-bases have been extensively employed and a large variety of planar macro-cyclic as well as macro-acyclic ligands have been synthesized to ascertain correctly the role of the different donor atoms, their relative positions, the number and size of the chelating rings formed, the flexibility and the shape of the coordinating moiety on the selective binding of charged or neutral species.

In 2008, Thakurta et al. reported [10] two new Cu(II) linear trinuclear Schiff base complexes, $[Cu_3L_2(CH_3COO)_2]$ (1) and $[Cu_3L_2(CF_3COO)_2]$ (2), using a symmetrical Schiff base ligand H_2L [where H_2L = N,N'-bis(2-hydroxyacetophenone)

propylenediimine]. Single-crystal X-ray structures shown that the adjacent Cu(II) ions are linked by doubly phenoxo bridges and a μ^2-η^1:η^1 carboxylato bridge [Fig. 5(a)]. In each complex, the central copper atom is located in an inversion centre with distorted octahedral coordination geometry, while the terminal copper atoms have square-pyramidal geometry.

Cryomagnetic susceptibility measurements over a wide range of temperature exhibit a distinct antiferromagnetic interaction of J = -36.5 and -72.3 cm^{-1} respectively [Fig. 5(b)]. Earlier Bag et al. reported [11] the first thermally-stable single oxo-bridged di-nuclear higher oxidation state Ni(III) complex [Fig. 6(a)].

Usually M-O-M type complexes, where M has d^n type of configuration with n > 5 are unstable due to the presence of electrons in the higher antibonding orbitals. In 2003, Choudhury et al. reported [12] first kind of singly phenoxo-bridged copper(II) dimeric complexes [Fig. 6(b)]. In this paper they established the interesting nature of variation of bridging modes of a Schiff-base within the same molecular system. They prepared complexes having the general formula: $[Cu_2(L)_2(XXX)(H_2O)](ClO_4)$, where L = a condensation product of o-vanillin and N,N-dimethylethylenediamine and XXX = SCN-, N^{3-} and NCO-. In the same year, Datta et al. published
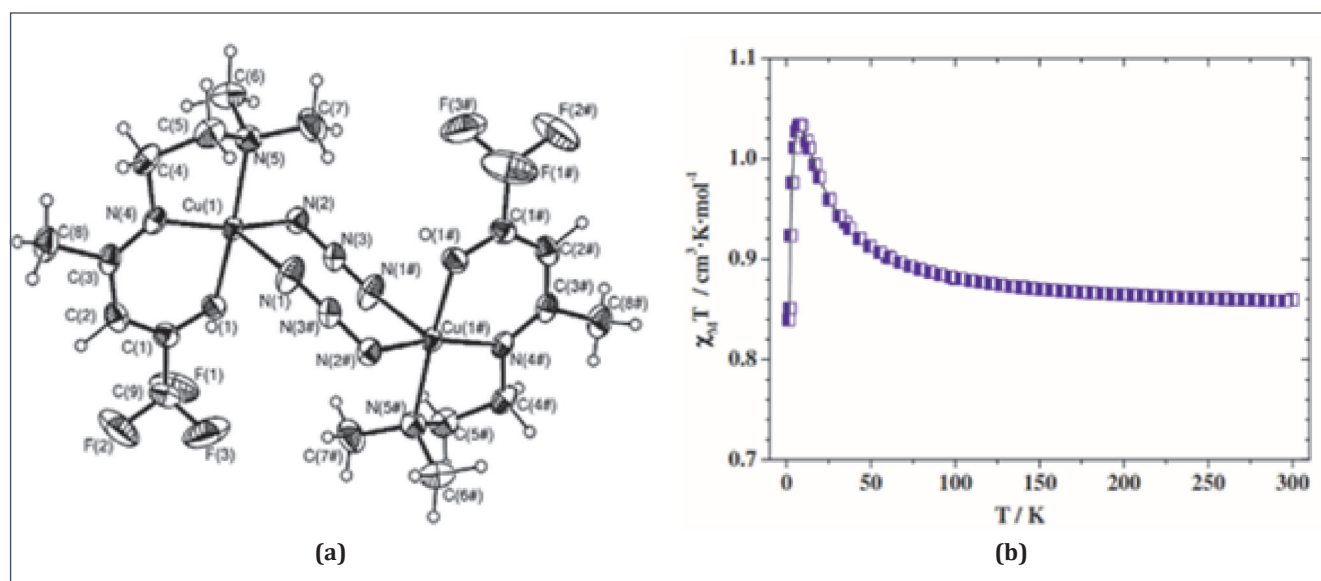

(a)   (b)

Fig. 4 : (a) End-to-End doubly azido bridged Cu(II) complex; (b) Temperature dependence of magnetic
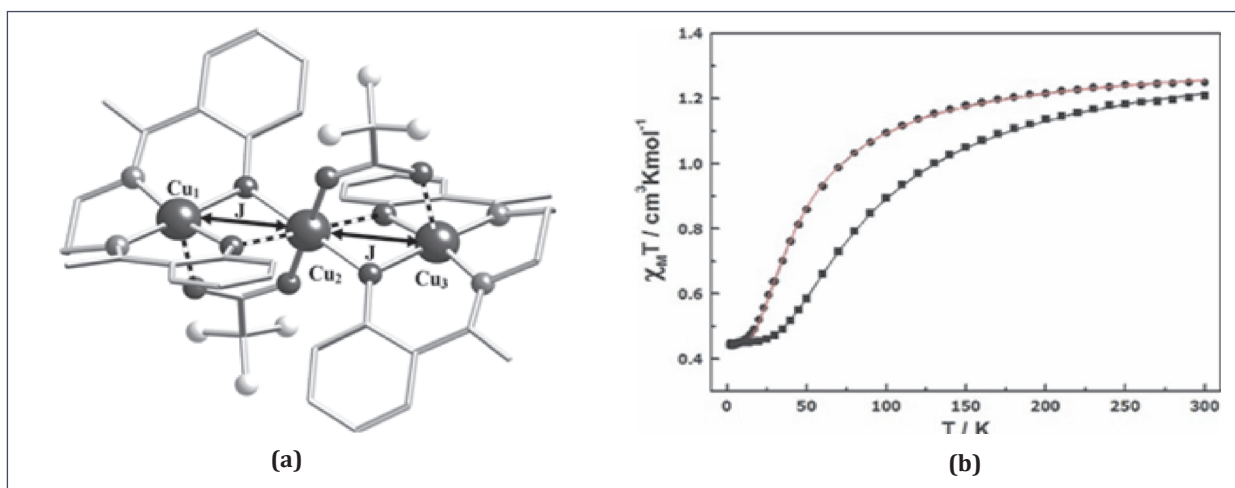
Fig. 5: (a) Schiff base and doubly carboxylato bridged Cu(II) trimeric complex; (b) Temperature dependence of magnetic susceptibility
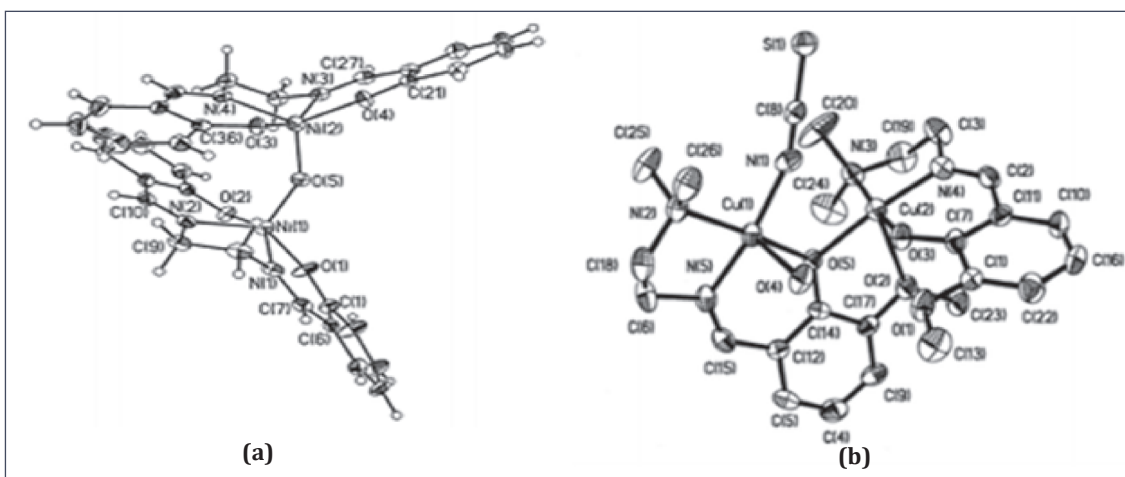

Fig. 6 : (a) Single oxo-bridged dinuclear Ni(III) complex; (b) ORTEP view of [Cu₂L₂(SCN)(H₂O)](ClO₄)

[13] another interesting novel doubly-phenoxo bridged linear Cu(II) trimer having the general formula, $Cu_3(L)_2(ClO_4)_2$ where L = a condensation Schiff-base product of 2-hydroxyacetophenone and 1,3-diaminopropane [Fig. (a)]. More recently Oshio *et al.* in 2004 published [14] a very noteworthy work on Single-molecule magnets of ferrous cubes [Fig. 7(b)] keeping a very good example of structurally controlled magnetic anisotropy. They successfully prepared six tetrameric ferrous cubes namely $Fe_4(L)_4(CH_3OH)_4$ [where L = sap, 5-Br-sap, sae, 5-Br-sae, 3,5-Cl₂-sae] and performed cryomagnetic measurements on them. Several other interesting homo- or heterometallic Schiff-base metal cubanes are also reported in the literature with their special magnetic behaviours.

5. Scope of Further Research

Inorganic crystal engineering is the modelling, synthesis and evaluation of the properties of crystalline materials obtained from inorganic, organo-metallic and bio-inorganic building blocks. The systematic investigation of coordination-polymers was the first foray into inorganic supra-molecular synthesis: in these systems multi-dentate ligands connect metal ions into infinite polymeric assemblies – the 'supra-molecular glue' is the coordinate-covalent bond. The resulting networks extend in directions dictated by the coordination geometry of the metal centre; thus, to create 1-D (e.g. chains), 2-D (e.g. square or hexagonal grids) or 3-D (e.g. diamondoid or cubic lattices) structures one must choose
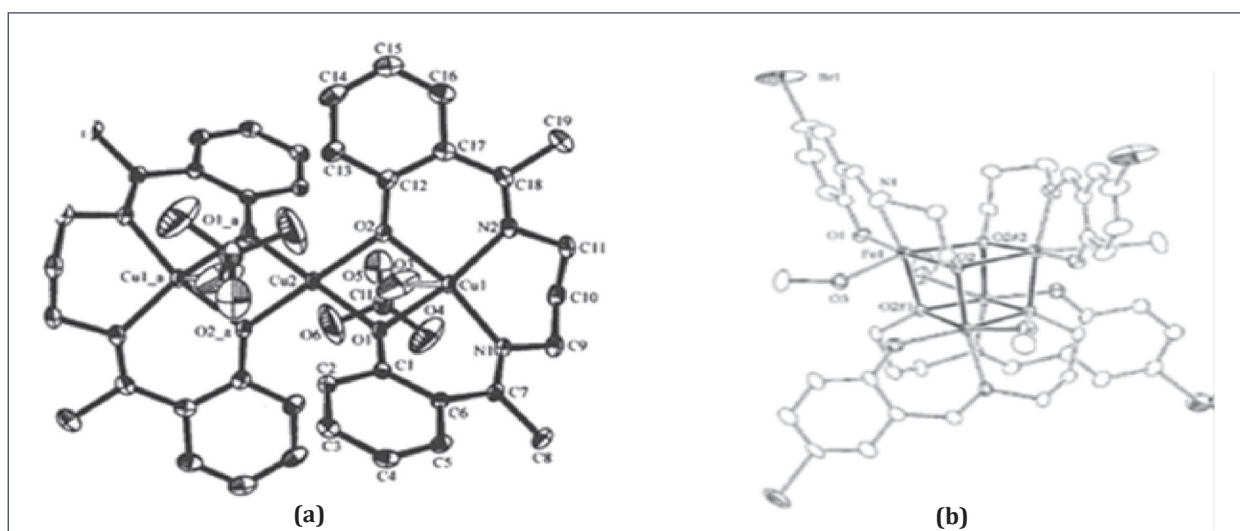
Fig. 7 : (a) Macrocylic Schiff-base coordinated tetra(μ-phenoxo) bridged trimeric linear Cu(II) complex; (b) ORTEP view of Fe$_4$(5-Br-sap)$_4$(CH$_3$OH)$_4$ single molecule magnet

the appropriate combination of metal ion and bridging ligand. The actual impact of inorganic and co-ordination chemistry is probably the true novelty in the field. Inorganic crystal engineering (ICE) uses transition metal and main group atoms, thus implying the whole periodic table of the elements. A corollary to this expansion is that the roles of charge, dipolar interactions, spin states, orbital levels and all the implications in terms of magnetism, charge transfer, spectroscopy, etc. need to be taken into account. Clearly, the number of combinations is limited only by the imagination of the researcher but also by what Nature can be induced to accommodate. Taking inspiration from the examples biology provides for the organisation of simple units into a vast range of intricate and beautiful structures with complex and wonderfully efficient functions, many chemists have been turning their attention to the deliberate design of self-assembling aggregates of molecular building blocks with some specific structural or functional purpose in mind.

6. Conclusion

It is difficult to give a full account of the development in this field, as the contribution by a large number of pioneers and excellent performers has come over a long period of time. As a result, only a few relevant scattered examples have been cited here. These Schiff-base complexes

may be good building blocks for the preparation of molecule-based magnets having customised magnetic properties.

7. References

[1] Desiraju, G. R. *Nature* **2001**, *412,* 397.

[2] Coronado, E.; Galan-Mascaros, J. R.; Gomez-Garcia, C. J.; Laukhin, V. *Nature* **2000**, *408,* 447.

[3] Miller, J. S.; Ed. *Magnetism: Molecules to Materials IV;* Wiley-VCH: Weinheim, Germany, **2003**.

[4] Chakraborty, J.; Thakurta, S.; Pilet, G.; Luneau, D.; Mitra, S. *Polyhedron* **2009**, *28,* 819.

[5] Shit, S.; Salah El Fallah, M.; Talukder, P.; Chakraborty, J.; Pilet, G.; Mitra, S. *Polyhedron* **2007**, *26,* 1357.

[6] Wen, H.-R.; Wang, C.-F.; Song, Y.; Zuo, J.-L.; You, X.-Z. *Inorg. Chem.* **2005**, *44,* 9039.

[7] Escuer, A.; Font-Bardia, M.; Penalba, E.; Solans, X.; Vicente, R. *Inorg. Chim. Acta* **2000**, *298,* 195.

[8] Li, L.; Jiang, Z.; Liao, D.; Yan, S.; Wang, G.; Zhao, Q. *Transit. Metal Chem.* **2000**, *25, 630.*

[9] Maji, T. K.; Mukherjee, P. S.; Mostafa, G.; Boquera, J. C.; Chaud09huri, N. R. *Chem. Commun.* **2001**, *1012.*

[10] Thakurta, S.; Chakraborty, J.; Rosair, G.; Salah El Fallah, M.; Mitra, S. *Inorg. Chem.* **2008**, *47,* 6227.

[11] Bag, B.; Mondal, N.; Rosair, G.; Mitra, S. *Chem. Commun.* **2000**, 1729.

[12] Choudhury, C. R.; Dey, S. K.; Karmakar, R.; De, C.; Mitra, S. *New J. Chem.* **2003**, *27,* 1360.

[13] Datta, A.; Choudhury, C. R.; Talukder, P.; Mitra, S.; Matsushita, T. *J. Chem. Res.* **2003**, 642.

[14] Oshio, H.; Hoshino, N.; Ito, T.; Nakano, M. *J. Am. Chem. Soc.* **2004**, *126*, 8805.

****

Tata Steel to acquire SFML's ferro alloy assets in Odisha for Rs 155 cr

Steel major Tata Steel said it will acquire ferro alloys producing assets of Odisha-based Stork Ferro and Mineral Industries for Rs 155 crore in an all-cash deal.

In this regard, an Asset Transfer Agreement has been signed between the two companies, a regulatory filing said. Tata Steel, in the filing said that it "has...executed an Asset Transfer Agreement with Stork Ferro and Mineral Industries Private Limited (SFML) for acquisition of itemized assets to produce ferro alloys. The asset purchase transaction will be carried out for cash consideration of Rs 155 crore plus applicable tax. The transaction does not involve any share acquisition."

The acquisition will be completed within two months from the date of execution of the asset transfer agreement, the company said.

SFML has two 16.5 MVA furnaces with annual production capacity of 53 kilo tonne per annum (Ktpa) located at Balasore, Odisha. The acquisition will provide an inorganic growth opportunity for Tata Steel Limited to augment its ferro alloys processing capacities.

Business Standard

Steel, fuel prices to impact domestic steel demand in coming quarters: Steel Mint

The domestic steel demand is expected to take a hit in the coming quarters due to "very high steel prices" and continuously rising fuel prices, according to industry consultancy SteelMint India.

Steel prices in India are trading at an all-time high. While hot-rolled coil (HRC) is quoting in the range of Rs 76,000-77,000 per tonne, cold-rolled coil (CRC) is costing between Rs 85,000-86,000 per tonne. Rebar price stands at Rs 72,000-73,000 a tonne, SteelMint India said.

In the domestic market, prices of HRC in the first week of March were in the range of Rs 68,000-69,000 a tonne, while CRC was at Rs 73,000-74,000 per tonne. Rebar was costing about Rs 67,500-68,500 a tonne. SteelMint said it "expects demand to be negative in coming quarters on rising steel prices and higher fuel prices, which may defer buying activities".

Financial Express

JSW Steel output jumps 21 pc to 1.58 Mt in February

JSW Steel registered a 21 per cent year-on-year (y-o-y) jump in its crude steel production to 1.58 million tonnes (Mt) for February. In a statement, the JSW Group company said its output had stood at 1.31 Mt in February 2021.

JSW Steel's production of flat-rolled products rose 25 per cent to 1.15 Mt in February 2022, compared with 0.93 Mt in the year-ago period. Its output of long-rolled products stood at 0.37 Mt, an eight per cent rise compared with 0.34 Mt a year ago.

The Economic Times

FORM IV

*Statement about ownership and other particulars about newspaper (**IIM Metal News**) to be published in the first issue every year after the last day of February*

1. Place of publication : The Indian Institute of Metals, "Metal House", Plot 13/4, Block-AQ, Sector-V, Salt Lake, Kolkata - 700 091

2. Periodicity of its publication : Monthly

3. Printer's Name : Print Max
   Nationality : Indian
   Address : 44, Biplabi Pulindas Street, Kolkata - 700 009

4. Publisher's Name : Shri Kushal Saha, Secretary General, IIM
   Nationality : Indian
   Address : The Indian Institute of Metals, "Metal House", Plot 13/4, Block-AQ, Sector-V, Salt Lake, Kolkata - 700 091

5. Editor's Name : Dr. N Eswara Prasad
   Nationality : Indian
   Address : The Indian Institute of Metals, "Metal House", Plot 13/4, Block-AQ, Sector-V, Salt Lake, Kolkata - 700 091

6. Names and addresses of individuals who own the newspaper and partners or shareholders holding More than one per cent of the total capital : Not Applicable

I, Kushal Saha, hereby declare that the particulars given above are true to the best of my knowledge and belief.

Date 28.03.2022   Signature of Publisher

****

Sambalpur Chapter

IIM Sambalpur Chapter organised a quiz contest through virtual mode on February 7, 2022 for the students of VSSUT Burla, which is the student chapter under Sambalpur chapter. The theme of the event was "Geek-O-Pedia 2022". The Winners were felicitated in the presence of Hon. Mr. S K Badjena, Head of the Department, Metallurgy and Material Science, VSSUT Burla on 8th March 2022 at VSSUT Burla, Sambalpur. The students were briefed about benefits of being the member of IIM and about Sambalpur Chapter.

Rourkela - Student Affiliate Chapter

IIM Rourkela Student Affiliate Chapter organised the Distinguished Lecture on "Tuning Structure and Properties of High Performance Metastable Alloys for Engineering Applications" on 28th February, 2022 at 06:00 pm (IST). The lecture was delivered by Prof. Jurgen Eckert, Materials Physics of the University of Leoben, Austria. Design perspective, fabrication techniques of metastable alloys, structure and thermodynamic parameters to control the properties were discussed in the lecture. The speaker's introduction and vote of thanks was given by Prof. Anshuman Patra (Metallurgical and Materials Engineering, NIT Rourkela) (Faculty Advisor of Indian Institute of Metals Student Affiliate Chapter). The lecture duration was around 50 minutes followed by discussions for around 15 minutes. The total views of the distinguished lecture in YouTube were around 115.

****

EDITORS	CORRESPONDENTS
Dr Monojit Dutta	Dr Chiradeep Ghosh (Jamshedpur)
Prof J Dutta Majumdar	Sri Rishabh Shukla (Pune)
Dr R Raghavendra Bhat	Dr Ramen Datta (Delhi)
Prof Sudhanshu Shekhar Singh	Dr L Ramakrishna (Hyderabad)
Dr Mithun Palit	Sri Lalan Kumar (Visakhapatnam)
	Sri A S Parihar (Kanpur)

ADVERTISERS' INDEX	
Name of the Organisations	*Page Nos.*
Durgapur Steel Plant	2nd Cover
PTC Industries Limited	5
Pragati Defence Systems Pvt Ltd	33
Tata Steel Ltd	34
JSW Steel Ltd	3rd Cover
Chennai Metco Pvt Ltd	4th Cover

![Pragati Defence logo]

Single action
QUICK RELEASE
OVERVEST with quick reassembly

Very simple and intuitive quick release system - easy to don or doff the vest in split seconds

Activated safety mechanism to prevent accidental release of vest

40% lighter protection from handgun ammunition, RCC's and FSP's with improved energy absorption and dissipation levels

Optional stab protection

Front, back and side protection

Detachable neck, shoulder, groin protection

COMFORTABLE &
ERGONOMIC DESIGN

30% thinner, 50% more flexible

Ergonomic and extremely comfortable design

Rifle butt rests for added comfort

No metal parts for added security

We make the best, even better.

JSW – A conglomerate worth $13 Billion believes in transformation to make a better world every day

It takes a strong will to be ranked among India's top business houses. But it was stronger dreams and ambition that made us venture into the core sectors of Steel, Energy, Cement and Infrastructure. Our strength, state-of-the art technology and excellence in execution have helped us grow and that has helped India grow multi-fold. By harbouring dreams of transformation, focusing on sustainability and a philosophy; to give back to the country, the JSW Group is making a better world every day.

Steel | Energy | Infrastructure | Cement | Paints
Realty | Ventures | Foundation | Sports
www.jsw.in

JSW
Better Everyday